

Accepted for Publication in the *Astronomical Journal* on
10/18/2005

A *Spitzer* Space Telescope Infrared Survey of Supernova Remnants in the Inner Galaxy

William T. Reach, Jeonghee Rho, Achim Tappe, Thomas G. Pannuti

Spitzer Science Infrared Center, California Institute of Technology, Pasadena, CA 91125

Crystal L. Brogan

Institute for Astronomy, University of Hawaii, 640 N. A'ohoku Place, Hilo, HI 96720

Edward B. Churchwell, Marilyn R. Meade, Brian Babler

*Department of Astronomy, University of Wisconsin, 475 N. Charter Street, Madison, WI
53706*

Rémy Indebetouw

Astronomy Department, University of Virginia, Charlottesville, VA 22904

Barbara A. Whitney

Space Science Institute, Boulder, CO 80303

reach@ipac.caltech.edu

ABSTRACT

Using Infrared Array Camera (IRAC) images at 3.6, 4.5, 5.8, and 8 μm from the GLIMPSE Legacy science program on the *Spitzer* Space Telescope, we searched for infrared counterparts to the 95 known supernova remnants that are located within galactic longitudes $65^\circ > |l| > 10^\circ$ and latitudes $|b| < 1^\circ$. Eighteen infrared counterparts were detected. Many other supernova remnants could have significant infrared emission but are in portions of the Milky Way too confused to allow separation from bright H II regions and pervasive mid-infrared emission from atomic and molecular clouds along the line of sight. Infrared emission from supernova remnants originates from synchrotron emission, shock-heated dust, atomic fine-structure lines, and molecular lines. The detected remnants are

G11.2-0.3, Kes 69, G22.7-0.2, 3C 391, W 44, 3C 396, 3C 397, W 49B, G54.4-0.3, Kes 17, Kes 20A, RCW 103, G344.7-0.1, G346.6-0.2, CTB 37A, G348.5-0.0, and G349.7+0.2. The infrared colors suggest emission from molecular lines (9 remnants), fine-structure lines (3), and PAH (4), or a combination; some remnants feature multiple colors in different regions. None of the remnants are dominated by synchrotron radiation at mid-infrared wavelengths. The IRAC-detected sample emphasizes remnants interacting with relatively dense gas, for which most of the shock cooling occurs through molecular or ionic lines in the mid-infrared.

Subject headings: shock waves, supernova remnants, infrared: ISM

1. Introduction

Much of the radiation from supernova remnants is expected to be emitted in the infrared range, from heated grains and nebular emission lines. However, supernova remnants have generally proven to be difficult to detect in the infrared, especially in the galactic plane where H II regions are far brighter. Two attempted infrared supernova remnant surveys used IRAS observations at 12–100 μm and found possible emission from 12 and 14 remnants (Arendt 1989; Saken, Fesen, & Shull 1992), respectively, with only 7 in common between the two surveys, from the sample of 95 remnants in the portion of the Galactic plane covered in the new survey presented in this paper.

We present in this paper a new infrared survey of supernova remnants using the Infrared Array Camera (IRAC) (Fazio et al. 2004) on the *Spitzer* Space Telescope (Werner et al. 2004). In the Galactic Legacy Infrared Mid-Plane Survey Extraordinaire (GLIMPSE) (Benjamin et al. 2003), the four IRAC arrays—with filters centered at 3.6, 4.5, 5.8, and 8 μm and pixels of 1.22'' size—were used to map the inner galaxy within galactic longitudes $65^\circ > |l| > 10^\circ$ and latitudes $|b| < 1^\circ$. GLIMPSE is a significant advance both because of the large increase in angular resolution and sensitivity as well as covering a new set of infrared wavelengths. There are 95 supernova remnants within GLIMPSE as per the Green (2004) catalog. The 5- σ sensitivity of GLIMPSE for point sources is 14.0, 12.0, 10.5 and 9.0 mag at 3.6, 4.5, 5.8, and 8 μm , respectively. The raw (1- σ) surface brightness sensitivity is 0.3, 0.3, 0.7, and 0.6 MJy sr⁻¹ at 3.6, 4.5, 5.8, and 8 μm , respectively. At 5.8 and 8 μm , most of the galactic plane is filled with diffuse emission, and at 3.6 and 4.5 μm point-source confusion is significant over much of the galactic plane. Thus the primary limitation of this supernova remnant survey is not instrumental noise but rather confusion from other, overlapping astronomical sources.

2. Infrared emission from supernova remnants

To provide a basis for comparison and possible classification of the infrared colors, we consider here the emission mechanisms expected to dominate the mid-infrared. Figure 2 summarizes the predictions in a color-color diagram.

Shocked gas cools through emission lines, and many important emission lines occur in the mid-infrared. The dominant coolant for shocked molecular gas, over a wide range of densities, is H₂ line emission. Fast shocks into moderately dense gas (e.g. 100 km s⁻¹ shocks into gas with density 10²⁻³ cm⁻³), cool via atomic fine-structure lines, for which we used a periodic table for fine structure lines to determine which should be the brightest (Reach et al. 2000). The following lines may be significant (in the indicated channel), **bold** for the brightest: H II(8-5) 3.74 μm (channel 1), **Brα 4.05 μm (channel 2)**, H II(8-6) 4.65 μm (channel 2), **Fe II 5.34 μm (channel 3)**, Ni II 6.64 μm (channel 4), **Ar II 6.99 μm (channel 4)**, Pfa 7.46 μm (channel 4), and Ar III 8.99 μm (channel 4). For the mature supernova remnant 3C 391 with shocks into moderately dense ($n \sim 10^2$ cm⁻³) gas, the 5-15 μm spectrum showed very bright Fe II and Ar II, in addition to H₂ lines (Reach et al. 2002). For the very young supernova remnant Cas A, which is dominated by ejecta and freshly-formed dust, the 6-16 μm spectrum showed very bright Ar II and Ar III (Arendt et al. 1999). For the supernova remnant RCW 103, a wide range of lines was detected over the wavelengths relevant to IRAC: H₂ lines in all channels, Brα in channel 2, Fe II in channel 3, Ar II and Ar III in channel 4 (Oliva et al. 1999).

Except for the youngest ($< 10^3$ yr), supernova remnants are dominated by swept-up interstellar matter, for which infrared emission from dust is inevitable, but the amount and color are not straightforward to predict. Mid-infrared emission from the interstellar medium is dominated by polycyclic aromatic hydrocarbon (PAH) bands, especially in the IRAC 5.8 and 8 μm channels. Figure 1 shows the spectrum of the reflection nebula NGC 7023, illustrating how typical interstellar dust may contribute to the IRAC wavebands. Grains are sputtered and vaporized in very strong shocks (Jones, Tielens, & Hollenbach 1996), which will reduce the infrared emission per unit mass. More importantly, in attempting to relate infrared features to the supernova remnants, grains are shattered in strong shocks (Jones, Tielens, & Hollenbach 1996). A size distribution with enhanced smaller grains will have a higher color temperature, because the smaller grains are out of thermal equilibrium and emit over a wide range of higher temperatures (Draine & Lee 1984). The smallest grains, or macromolecular PAH may be destroyed or altered in even slower shocks and are largely absent in dense, shocked clumps (Reach et al. 2002). Thus it is nearly impossible to predict the colors of supernova remnants at IRAC wavelengths: the processes are too complicated (and in competition with each other), and the shocks span too wide a range of properties for

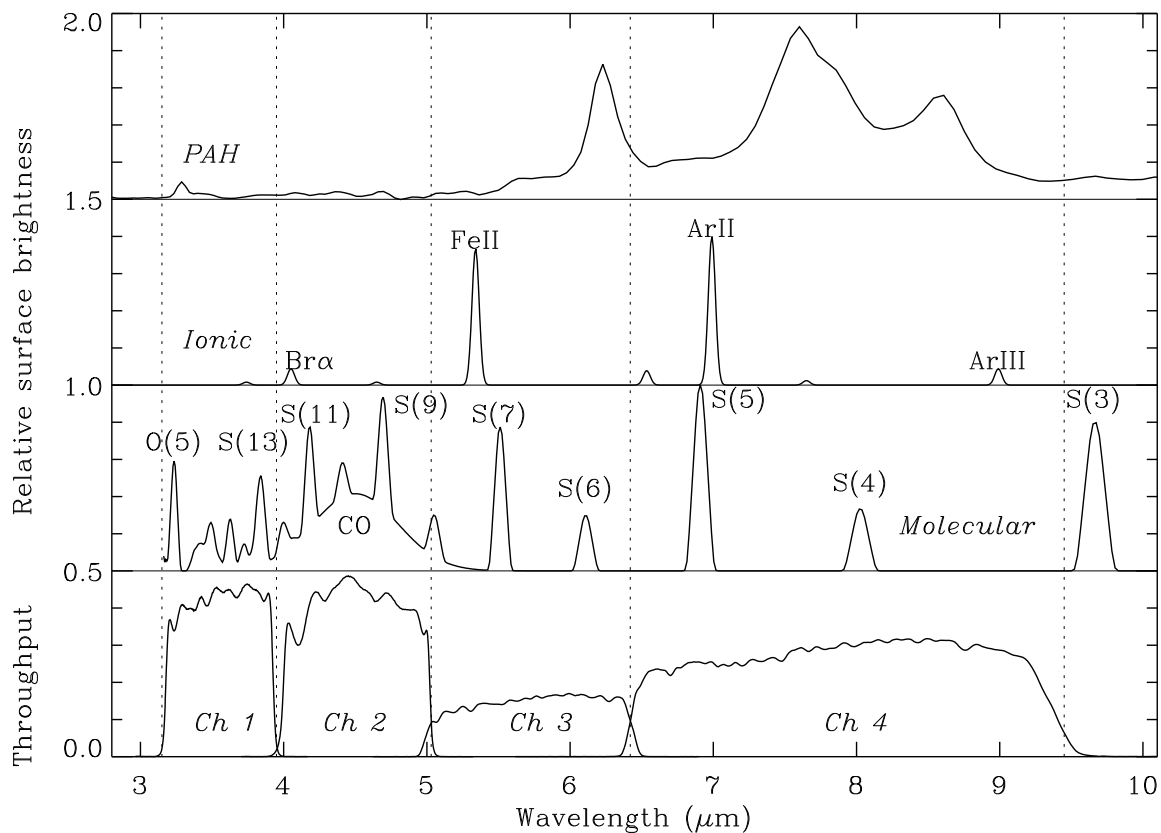


Fig. 1.— *Spitzer*/IRAC spectral response compared to 3 template spectra. The top curve is the *ISO*/*SWS* spectrum of NGC 7023, dominated by PAH emission bands; the second from top is a combination of lines expected from cooling, ionized gas behind a fast shock; the third from top is a combination of H_2 lines and the CO fundamental band. The lower portion shows the spectral response for each IRAC channel.

there to be a typical color. Diffuse interstellar clouds have a wide range of 12/100 μm ratios—possibly due to shock processing by prior supernova blast waves. Given this range of possible initial conditions of the grains, it is even more unlikely that the processed grains will have predictable properties. That being said, observations of infrared emission from SNRs to date have shown little or no evidence of significant dust emission (PAH or continuum) within the wavelengths of the IRAC bands. We expect shocked dust to contribute more in the longest-wavelength IRAC channel than the others, whether the emission is from macromolecular PAH or from small grains.

Synchrotron emission can contribute to all wavelengths from the radio to X-ray, and has been detected in the near-infrared from Cas A (Rho et al. 2003). The color of pure synchrotron emission in the IRAC bands would be approximately 0.6/0.7/0.8/1. None of the supernova remnants we detected have this color. The one with colors closest to pure synchrotron is for a line of sight for which the mid-infrared spectrum was measured with *ISO* and was dominated by molecular line emission with negligible continuum (?). Since many of the SNR in our sample are very bright in the radio, we expect them to all have at least faint synchrotron radiation. The expected effect of this synchrotron radiation on the mid-infrared colors is to ‘fill in’ the channels that do not have significant line or dust emission.

Simple models are presented below for the mid-infrared colors expected from the three main SNR emission mechanisms described above. A summary of the derived color/emission mechanism templates is presented in Figure 2.

We now develop simple models to generate template colors for the three main emission mechanisms.

ISM—First, for the reflection nebula NGC 7023, the colors in the IRAC channels 1/2/3/4 are 0.054/0.061/0.40/1. For the H II region NRAO 530 (as measured from the Spitzer/IRAC/GLIMPSE data near the supernova remnant 3C 396), the mid-infrared colors are 0.040/0.046/0.35/1 (using the same proportion notation for channels 1/2/3/4, wavelengths 3.6/4.5/5.8/8 μm , which will be used throughout this paper). The origin of these colors is a combination of PAH and nebular line emission, probably with a large PAH contribution based on the similarity to NGC 7023. The H II region and reflection nebula colors are very similar and will be difficult to distinguish, but for our purpose of classifying unprocessed interstellar medium this is not important. Figure 2 shows the colors of NGC 7023 and outlines a region of color-color space that could be attributed to sources with similar spectra.

Shocked molecules—The colors of a source dominated by molecular emission lines can be estimated using a three-temperature-component H_2 excitation model that matches many lines over a wide range of energy levels for IC 443 (Rho et al. 2001). The IRAC colors of a shocked

H₂ clump are expected to be 0.42/0.52/0.90/1. Note the significantly enhanced emission in channels 1 and 2. Furthermore, there is a CO fundamental band that falls within channel 2, with total emission comparable to that of H₂ in Herbig-Haro shocks with similar densities and shock velocities. Thus a shocked H₂+CO clump would have colors 0.42/1/0.90/1. The strong channel 1+2 enhancement turns out to be a key to distinguishing supernova remnants interacting with molecular gas from the unrelated interstellar medium or ionized gas. To allow for variations in the H₂ excitation compared to that seen in IC 443, we computed models for a range of gas temperatures (> 1000 K) and combinations of temperature components that yield at least some of the lines observed toward IC 443, RCW 103, or HH objects. The infrared emission of two survey remnants (W 44 and 3C 391) for which we have narrow-band H₂ images are discussed in §4, validating the usage of IRAC colors to identify shocked molecular gas.

Ionized gas—Pure, ionized hydrogen would have IRAC colors 0.25/3.7/0/1, including the Br and Pf lines listed above, assuming case B recombination at 10⁴ K (Osterbrock 1989). However there will always be some heavier elements in Galactic regions. We consulted a periodic table for fine structure lines (Reach et al. 2000) and used the observed line ratios for RCW 103 from spectroscopy with the *Infrared Space Observatory* (Oliva et al. 1999) as a guide to the brightness relative to Br α . Including lines of H, Fe⁺, Ni⁺, Ar⁺, and Ar⁺⁺, the predicted colors for ionic shocks is 0.01/0.10/0.74/1. Such gas is distinguishable from unshocked ISM and shocked molecular gas by its bright channel 3 and very faint channel 1. Figure 2 shows the predicted IRAC colors of RCW 103, together with a rectangular region that bounds similar regions. The predicted and observed colors are discussed in the section on RCW 103 below. Note that if the shocks destroy grains more or less efficiently as in RCW 103, then channel 3 will increase or decrease significantly, because Fe II is the dominant ionic contribution to channel 3.

For stellar ejecta, the colors are more difficult to predict and can have a wide range. The infrared colors of young SNRs are expected to vary from SNR to SNR because the contribution and composition of ejecta depend on a number of physical parameters such as the type of progenitor star, amount of the enriched metal abundances and the degree of particle acceleration. For illustration, the ISO spectra of Cas A show little or no [Fe II] emission, which would move sources vertically in Figure 2. And compared to RCW 103, Cas A has little H II emission, which moves points to the left in Figure 2. From archival ISO data (including TDT 7510064320), the spectrum of Cas A shows no bright continuum over the IRAC wavelengths, and only one bright line ([Ar II] 6.99 μ m); the IRAC colors based on the detected spectral lines would be 0.01/0.03/0.18/1, with the paucity of channel 1 and 2 emission due to no bright ionic lines in channel 1 and little expected Br α in channel 2 (due to low H abundance). In Figure 2, the Cas A spectrum falls to the left of the ‘Ionic’ region,

but below the ‘PAH’ region. None of the supernova remnants we detected in this survey have the colors of synchrotron emission.

The infrared emission of the survey remnants 3C 391, W 44, 3C 397, and W 49B, for which we have narrow-band images in near-infrared Fe II and H₂ filters, is discussed in §4, validating the usage of IRAC colors to identify emission from ionic shocks and to distinguish them from molecular shocks.

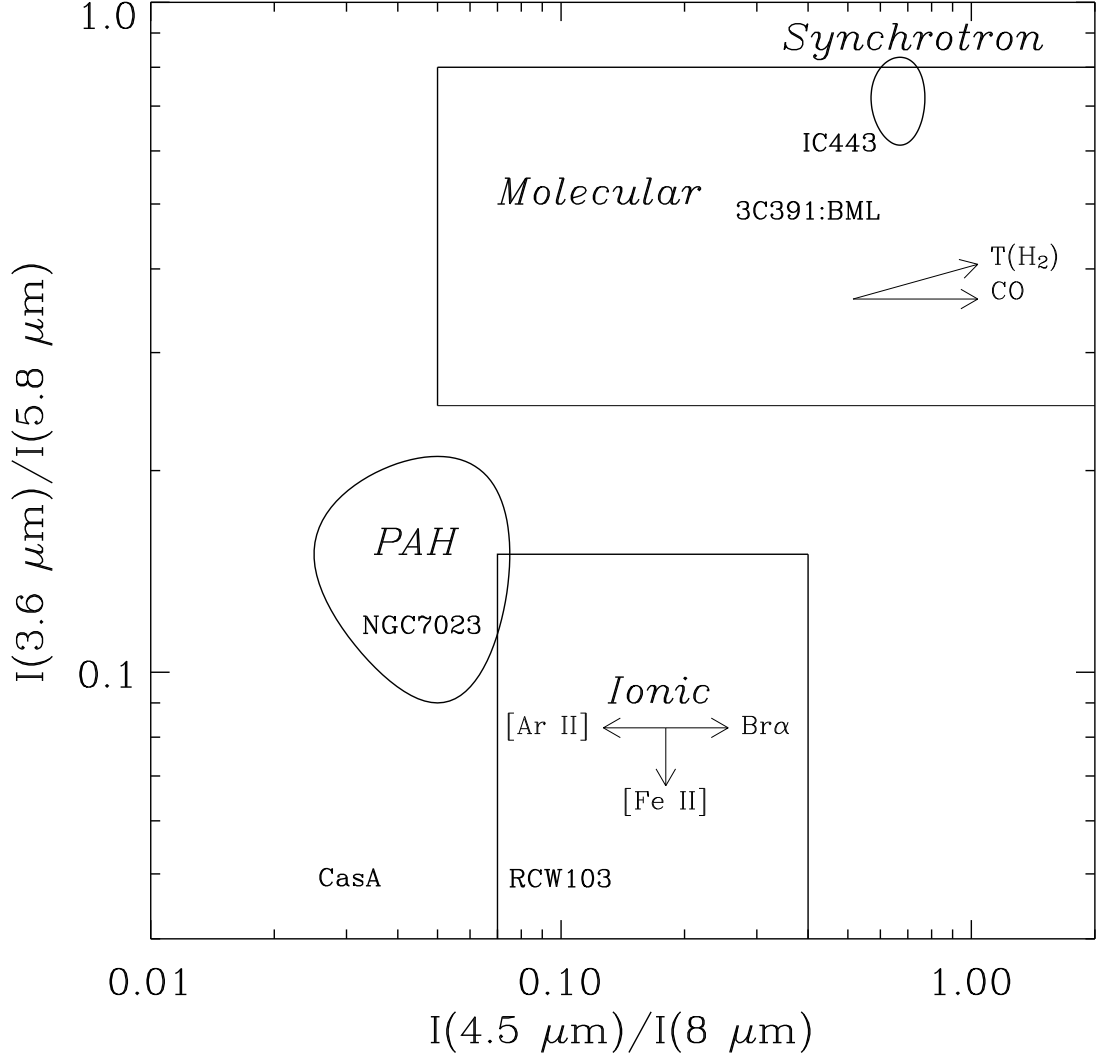


Fig. 2.— Schematic IRAC color-color diagram showing the predicted colors of the main emission mechanisms expected for supernova remnants in the mid-infrared: shocked molecular gas, shocked ionized gas, and photodissociation regions (PAH). The choice of color axes shown here separates the major emission mechanisms best. The boundaries delineate the approximate area occupied by a set of models for H₂ excitation and the colors inferred from observed spectra of photodissociation regions and ionic shocks. For molecular shocks two arrows indicate the color trends for increasing H₂ excitation, T(H₂), and CO vibrational emission. For ionic shocks, the arrows show the color trends of increasing Brα 4.05 μm, [Fe II] 5.35 μm, and [Ar II] 6.99 μm. The boundaries of the various emission mechanisms are intended to bound the expected range of physical conditions behind shock fronts. For the molecular shocks, a range of temperatures from 1000 to 2000 K, and mixtures with CO, are included. For ionic shocks, line ratios for RCW 103 were used as a basis and supplemented with line ratios for fainter lines in M 17. Material with unusual abundances, such as supernova ejecta or circumstellar material, can have unusual colors. Some of the template

3. Survey for infrared emission

Table 1 presents the list of supernova remnants contained within the boundaries of the infrared survey. The survey procedure is depicted in Figure 3. Each remnant was inspected visually on preliminary mosaics generated immediately upon release of the data by the Spitzer Science Center (SSC). Greyscale images at 4.5 and 8 μm were displayed with overlaid circles depicting the size and location of each remnant in the Green (2004) catalog. A preliminary score was assigned according to the following scheme: 1=likely detection (with infrared shells or other structures coinciding with radio, X-ray or optical structure, often with a color distinct from the diffuse interstellar medium), 2=possible detection (with some apparent relation between the infrared and radio image but indistinct colors and too much confusion with unrelated emission), 3=unlikely detection (but so much confusion with unrelated emission that there could be significant unrecognized emission from the supernova remnant), 4=not detected. Remnants with scores of 1 or 2 were selected for follow-up, and improved mosaics were generated for fields centered on each remnant. The improved mosaics were generated using the self-calibration mosaic technique, allowing for relative background offsets between images and a flat-field for the array to be determined simultaneously with the sky mosaic (Fixsen, Moseley, & Arendt 2000). Radio images were obtained from the Molonglo Observatory Synthesis Telescope (MOST) Supernova Remnant Catalog (Whiteoak & Green 1996), the National Radio Astronomy Observatory Very Large Array (VLA) Sky Survey (Condon et al. 1998), individual authors for some of the individual remnants described in the detailed notes below, or reprocessed VLA archival data for G11.4-0.1, 3C 391, 3C 396, 3C 397. The radio contours were superposed on the infrared images, both the three-color combination of 3.6 (blue), 4.5 (green), and 8 (red) μm , and a monochromatic 5.8 μm image. The revised probability of an infrared counterpart was then determined for each remnant. The score was 1 for cases where a clear association between the infrared emission and the radio emission could be made even if the association was not detailed, for the infrared morphology rarely matches the radio morphology. The score was 2 for remnants where there is infrared emission that is suggestive but cannot be convincingly associated with the remnant. Of the 95 remnants within the survey boundary, 18 were detected (score 1), and 17 were too confused (score 2). In this paper, we concentrate our discussion on remnants with score 1, but those with score 2 are worthy of future detailed studies.

Table 1. Supernova Remnants in the IRAC/GLIMPSE Survey

SNR	Name	Size(')	Detected? ^a	SNR	Name	Size(')	Detected? ^a
G11.2-0.3		4	1	G308.1-0.7		13	4
G11.4-0.1		8	3	G308.8-0.1		25	2
G12.0-0.1		7	3	G309.2-0.6		14	3
G13.5+0.2		5	3	G309.8+0.0		22	3
G15.9+0.2		6	3	G310.6-0.3	Kes 20B	8	2
G16.7+0.1		4	3	G310.8-0.4	Kes 20A	12	1
G18.8+0.3	Kes 67	14	3	G311.5-0.3		5	1
G20.0-0.2		10	3	G312.4-0.4		38	3
G21.5-0.9		4	3	G315.4-0.3		19	2
G21.8-0.6	Kes 69	20	1	G315.9-0.0		10	3
G22.7-0.2		26	1	G316.3-0.0	MSH 14-57	20	3
G23.3-0.3	W 41	27	2	G317.3-0.2		11	3
G23.6+0.3		10	3	G318.2+0.1		37	3
G24.7+0.6		21	3	G318.9+0.4		20	3
G24.7-0.6		15	4	G321.9-0.3		27	3
G27.4+0.0	4C-04.71	4	3	G322.5-0.1		15	3
G27.8+0.6		39	3	G323.5+0.1		13	2
G28.6-0.1		11	3	G327.4+0.4	Kes 27	21	2
G29.6+0.1		5	4	G328.4+0.2	MSH 15-57	5	4
G29.7-0.3	Kes 75	3	3	G329.7+0.4		36	2
G31.5-0.6		18	3	G332.0+0.2		12	4
G31.9+0.0	3C 391	6	1	G332.4-0.4	RCW 103	10	1
G32.1-0.9		40	3	G332.4+0.1	Kes 32	15	2
G32.8-0.1	Kes 78	17	3	G335.2+0.1		21	2
G33.2-0.6		18	3	G336.7+0.5		12	4
G33.6+0.1	Kes 79	10	2	G337.0-0.1	CTB 33	2	3
G34.7-0.4	W 44	31	1	G337.2-0.7		6	4
G36.6-0.7		25	2	G337.8-0.1	Kes 41	7	2
G39.2-0.3	3C396	7	1	G338.1+0.4		15	4
G40.5-0.5		22	4	G338.3-0.0		8	3
G41.1-0.3	3C397	4	1	G338.5+0.1		9	3
G42.8+0.6		24	4	G340.4+0.4		8	4
G43.3-0.2	W49B	4	1	G340.6+0.3		6	2
G45.7-0.4		22	2	G341.2+0.9		19	4
G46.8-0.3		15	3	G341.9-0.3		7	4
G49.2-0.7	W51C	30	3	G342.0-0.2		10	3
G54.1+0.3		2	3	G342.1+0.9		9	4
G54.4-0.3		40	1	G343.1-0.7		24	3
G55.0+0.3		17	2	G344.7-0.1		10	1
G57.2+0.8		12	4	G345.7-0.2		6	4
G59.5+0.1		5	3	G346.6-0.2		8	1
G296.1-0.5		32	3	G347.3-0.5		60	3
G296.8-0.3		16	3	G348.5+0.1	CTB 37A	15	1
G298.5-0.3		5	2	G348.5-0.0		10	1
G298.6-0.0		11	2	G348.7+0.3	CTB 37B	17	3
G299.6-0.5		13	3	G349.2-0.1		8	3

Table 1—Continued

SNR	Name	Size(')	Detected? ^a	SNR	Name	Size(')	Detected? ^a
G302.3+0.7		17	3	G349.7+0.2		2	1
G304.6+0.1	Kes 17	8	1				

^a Likelihood of mid-infrared counterpart for the SNR, determined by inspection of the IRAC data and comparison to existing radio images: 1=detected (18 objects), 2=possibly detected but confused (17 objects), 3=not detected but confused (44 objects), 4=not detected at GLIMPSE sensitivity (16 objects).

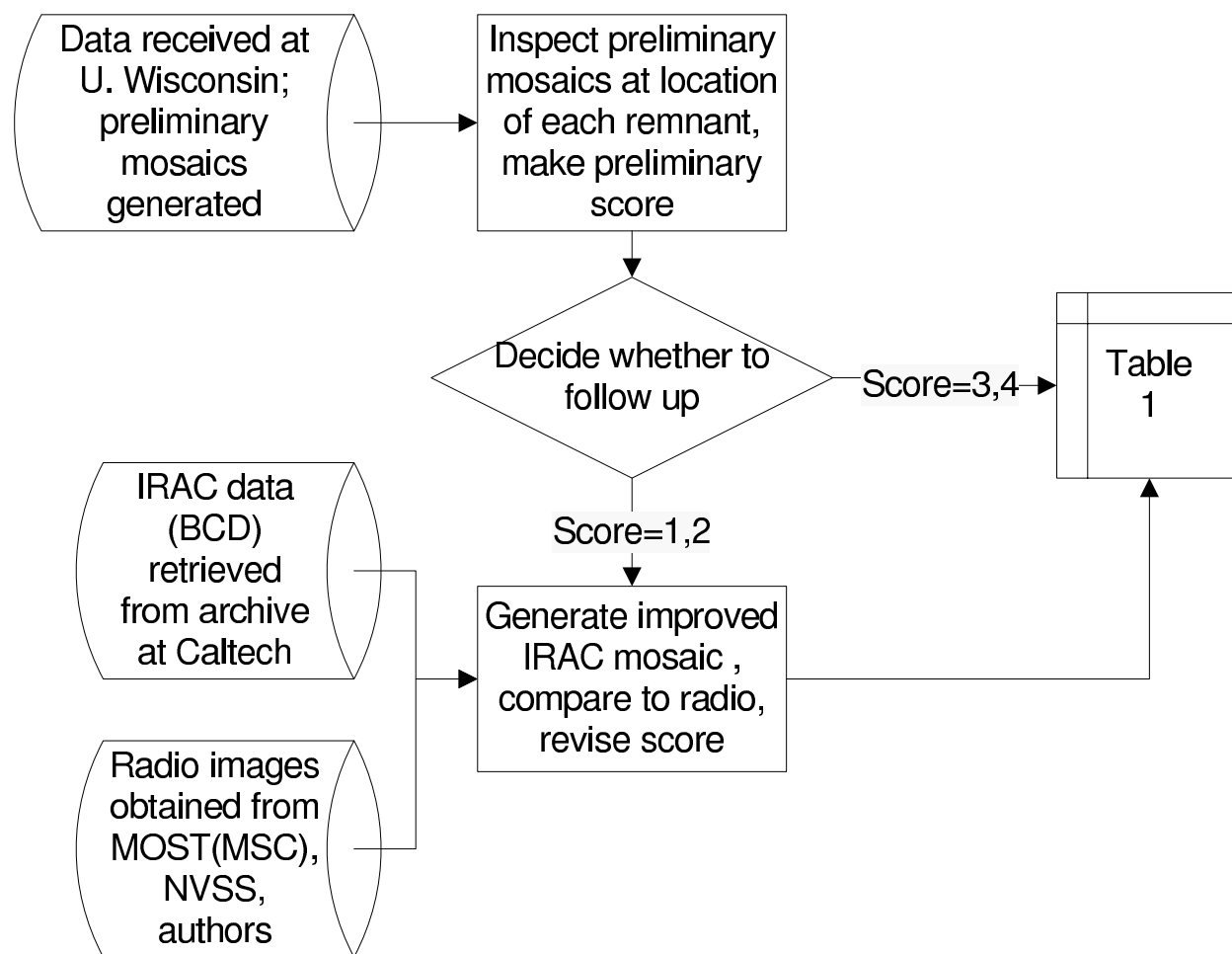


Fig. 3.— Flowchart of the Spitzer/IRAC/GLIMPSE galactic plane supernova remnant survey.

3.1. Comparison to previous surveys

For comparison, the *IRAS*-based survey by Arendt (1989) detected 12 (17%) of the remnants within the portion of the galactic plane included in the *Spitzer*/IRAC/GLIMPSE survey, and the independent *IRAS*-based survey by Saken, Fesen, & Shull (1992) detected 14 (18%). Only 7 (10%) of these remnants were detected in common by the two *IRAS*-based surveys: 3C 391, W 49B, G54.1+0.3, Kes 17, G315.4-0.3, G340.6+0.3, and G349.7+0.2. The new *Spitzer*/IRAC results presented here are a significant advance, primarily because of the increase in angular resolution, which allows better separation of stars, H II regions, and other interstellar clouds from the remnants. The present survey detects 6 remnants in common with Arendt (1989) and 4 remnants in common with Saken, Fesen, & Shull (1992). There are only 4 remnants in common among all 3 infrared surveys: 3C 391, W 49B, Kes 17, G349.7+0.2.

First, let us consider those supernova remnants apparently detected by *Spitzer* and *IRAS*. We compared the GLIMPSE images to the *IRAS* images from the Arendt (1989) catalog. The *IRAS* images of W 44, W 49B, and G349.7+0.2 contain emission plausibly associated with the remnant as traced by radio and *Spitzer* infrared images. For 3C 391, the 60 μm emission shows a believable emission peak from the remnant, while the other channels are clearly due to unrelated H II regions. For Kes 17 and G11.2-0.3, the structures in the *IRAS* images appear to be all due to unrelated H II regions, and their apparent detections are spurious: the dashed circles that indicate the region within which the fluxes were measured by Arendt (1989) contain bright H II regions that are clearly outside the radio shells.

As for the supernova remnants apparently detected by *IRAS* and not *Spitzer*, they are either so confused with H II regions (e.g. G12.0-0.1) that we cannot tell whether there are counterparts in either survey, or the *IRAS* detections (e.g. CTB 37B) are likely to be unrelated H II regions. In principle, some of the mismatches between *IRAS* and not *Spitzer* could be due to the difference in wavelength, since it is possible that the *IRAS* emission is from dust while the *Spitzer*/IRAC traces shocked gas; however, for the specific cases in the present survey. We attribute the differences between the *IRAS* and *Spitzer* surveys to be primarily due to contamination of the *IRAS* observations at low galactic latitudes. Other infrared surveys with higher angular resolution, for example 24 μm observations with *Spitzer* and future far-infrared observations with *Herschel* will likely detect many more counterparts.

4. Results for individual remnants

Table 2 lists the 18 remnants detected by the IRAC/GLIMPSE survey. Brief descriptions of the mid-infrared emission, and some relevant context, are given below for each detected remnant, with the subheading *bold* for detected (score 1) and *italics* for possibly-detected (score 2) remnants.

G11.2-0.3—This compact, circular SNR has a composite radio morphology, with a clearly-defined, steep-spectrum shell (brightest in the SE) combined with a flat-spectrum core. X-ray observations show a shell (with a thermal spectrum) similar to that seen in the radio; a centrally-located pulsar (AX J1811.5-1926) and a pulsar wind nebula are associated with the SNR (Kaspi et al. 2001). Some evidence indicates G11.2-0.3 is associated with the supernova of 386 AD, and the expansion of the remnant was detected by proper motion of the radio shell (Tam & Roberts 2003); both of these factors suggest this SNR is relatively young. The mid-infrared images (Figure 4a) reveal a thin filament with three bright segments located within the SE rim of the SNR. Figure 4b shows that the filaments correspond precisely with the two brightest segments of the SE X-ray rim. The filaments connect to a fainter extension along most of the eastern radio shell. More diffuse infrared emission is seen toward the eastern half of the SNR, though it is unclear if this emission is in fact associated with the SNR. No infrared emission is seen toward the NW quadrant of the SNR. There is no infrared emission associated with the pulsar wind nebula. The filament near $18^{\text{h}}11^{\text{m}}35.0^{\text{s}}-19^{\circ}26'23''$ is detected in channels 3 and 4 with comparable brightness in both channels (10 MJy sr^{-1}), but it is not seen in channels 1 or 2. The blob of emission at $18^{\text{h}}11^{\text{m}}31.5^{\text{s}}-19^{\circ}27'16''$ is detected in all 4 IRAC channels, with color ratios 0.3/0.7/1.1/1. The colors suggest the IRAC emission from the filaments is dominated by line emission from shocked gas and certainly not the PAH dust that dominates unshocked ISM. Since the remnant is young, some of the emission could also arise from ejecta.

Table 2. Properties of detected supernova remnants^a

SNR	Name	Diameter(')	region	3.6/8	4.5/8	5.8/8	I8 (MJy/sr)
G11.2-0.3		4	SE rim	0.34	0.48	0.58	7.5
G21.8-0.6	Kes 69	20	S ridge	< 0.14	0.91	1.4	2
G22.7-0.2		26	S boundary	< 0.07	< 0.07	0.37	23
G31.9+0.0	3C 391	6	BML/OH mas	0.18	0.36	0.67	23
			NW Fe/radio bar	< 0.14	0.41	1.7	5
G34.7-0.4	W 44	31	E shell	0.37	0.75	0.75	11
G39.2-0.3	3C 396	7	W shell	< 0.10	0.27	0.63	10
			central filament	< 0.07	0.04	0.37	27
G41.1-0.3	3C 397	4	N shell	< 0.07	0.14	0.73	8
G43.3-0.2	W 49B	4	Fe/radio hoop	0.08	0.46	1.0	8
			H ₂ filament	0.16	0.42	0.76	6
G54.4-0.3		40	N boundary	0.04	0.04	0.33	15
G304.6+0.1	Kes 17	8	filament	0.33	0.34	0.67	5
			shell	0.12	0.30	0.39	29
G310.8-0.4	Kes 20A	12	SE shell	0.18	0.18	0.61	15
G311.5-0.3		5	shell	0.41	0.54	0.91	9
G332.4-0.4	RCW 103	10	shell	0.19	0.38	0.79	15
			filament	< 0.07	0.14	0.59	10
G344.7-0.1		10	shell	< 0.20	0.23	0.82	10
G346.6-0.2		8	shell	0.23	0.41	0.61	6
G348.5+0.1	CTB 37A	15	N blob	0.11	0.32	0.52	24
			arc	0.07	0.04	0.42	62
G348.5-0.0		10	filament	0.14	0.29	0.64	14
G349.7+0.2		2	filament	0.05	0.14	0.59	170

^aThe columns 3.6/8, 4.5/8, and 5.8/8 are the ratio of the surface brightness in IRAC channels 1, 2, and 3 to IRAC channel 4. The emission was assumed to be spatially extended, so the colors measured from the images were multiplied by factors of 1.36, 1.36, and 0.91, respectively (Reach et al. 2005).

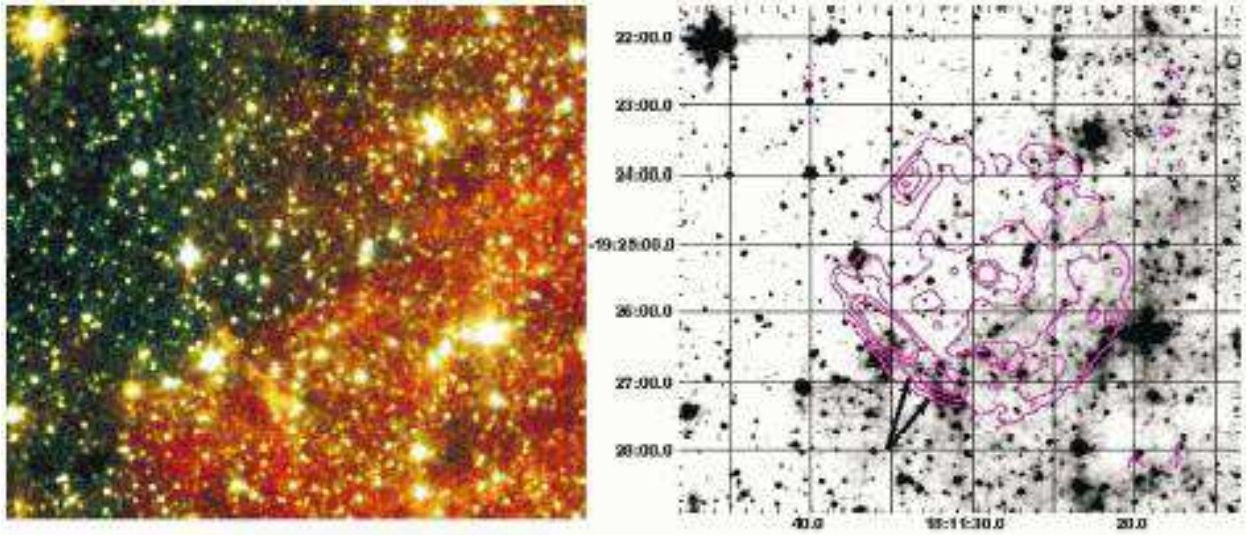


Fig. 4.— (a) *Spitzer*/IRAC color image of the supernova remnant G11.2-0.3. The colors are red= $8\mu\text{m}$, yellow= $5.8\mu\text{m}$, green= $4.5\mu\text{m}$, blue= $3.6\mu\text{m}$, magenta= $5.8\mu\text{m} - 0.32\times 8\mu\text{m}$. These IRAC images were adaptively smoothed to reduce noise while preserving angular resolution on bright features. (b) *Spitzer*/IRAC $5.8\mu\text{m}$ image of the supernova remnant G11.2-0.3. *Chandra* all-energy contours are superposed. Two infrared filaments are indicated (arrows). *NOTE: this figure was degraded in quality for distribution on astro-ph.*

Kes 69 (G21.8-0.6)— Figure 5 shows a prominent, ‘green’ ridge of mid-infrared emission, passing through $18^{\text{h}}30^{\text{m}}22.0^{\text{s}}-10^{\circ}15'41''$ in the southern radio shell. The IRAC color ratios are $(< 0.1)/0.67/1.5/1$, which are inconsistent with PAH emission. Channels 2 and 3 are most likely dominated by lines from shocked gas. The exceptionally bright channel 3 emission (relative to channel 4) could be due to a bright Fe II line, suggesting very efficient grain destruction in the shocks. The bulk of the radio emission of Kes 69 originates from the southeastern shell; likewise, the infrared emission originates from the same location. The X-ray emission, on the contrary, appears interior to the radio shell (Yusef-Zadeh et al. 2003). An OH maser has been detected from the northern part of Kes 69 (Green et al. 1997; Yusef-Zadeh et al. 2003); faint, diffuse mid-infrared emission, possibly unrelated to the SNR, is seen in the vicinity of the OH maser.

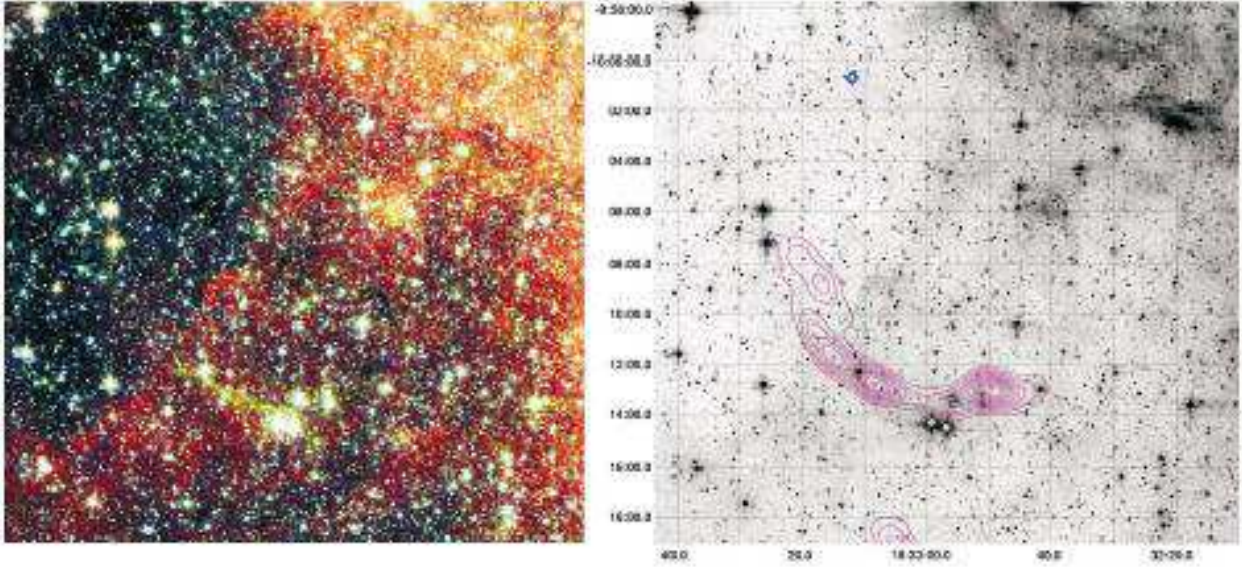


Fig. 5.— **(a)** *Spitzer*/IRAC color image of the supernova remnant Kes 69. The colors are red= $8\mu\text{m}$, yellow= $5.8\mu\text{m}$, green= $4.5\mu\text{m}$, blue= $3.6\mu\text{m}$. **(b)** *Spitzer*/IRAC $5.8\mu\text{m}$ image Kes 69 with radio (NVSS) contours superposed. The diamond in the NW is the position of an OH 1720 MHz maser. *NOTE: this figure was degraded in quality for distribution on astro-ph.*

G22.7-0.2—This remnant is located in a field with multiple H II regions and is adjacent to W 41. A very bright infrared region G22.75-0.25 ($18^{\text{h}}33^{\text{m}}46.5^{\text{s}}-09^{\circ}10'02''$) is located just E of the center of the remnant. This region is evident as a very bright compact source in the 1420 MHz NVSS (Condon et al. 1998) with flux ~ 100 mJy, but the source is not evident at 330 MHz (Kassim et al. 1992), suggesting it may be thermal emission from an H II region. Elsewhere along the supernova remnant shell there is a small probable H II region in the NE at G22.73-0.01 ($18^{\text{h}}32^{\text{m}}42.3^{\text{s}}-09^{\circ}04'43''$). A relatively unique region is located in the W shell at G22.78-0.40, ($18^{\text{h}}34^{\text{m}}12.7^{\text{s}}-09^{\circ}11'15''$). There are numerous mid-infrared filaments evident at 5.8–8 μm , and at least one with relatively bright 3.6–4.5 μm emission. The infrared emission is probably a mixture of PAH features and gas lines. The positional coincidence with the radio shell, filamentary morphology, and infrared colors lead us to suspect this is a supernova-cloud interaction region, but improved infrared images or other supporting evidence are needed to properly classify the nature of this region. There is a bright region of infrared emission in between G22.7-0.2 and the adjacent supernova remnant W 41. While this could be a coincidental projection effect, the location is very suggestive. This could be a case where an interstellar cloud is being ‘sandwiched’ with impacts from different supernova remnants (or the progenitors’ and cluster members’ winds) on either side. There is a general ‘deficit’ of infrared emission within the radio shell, clearly evident in Figure 6. The region of decreased infrared emission has a sharp boundary in the southern portion of the remnant, just south of the NVSS radio contours. The shape of the southern cavity boundary follows the shape of the remnant too closely to be a chance alignment. The colors of this southern rim are very red, possibly due to PAH emission. The morphology and colors suggest that the observed emission is not from strong shocks, but instead it may arise from a region evacuated by the progenitor (and possibly other cluster members) and currently illuminated by the remaining cluster members.

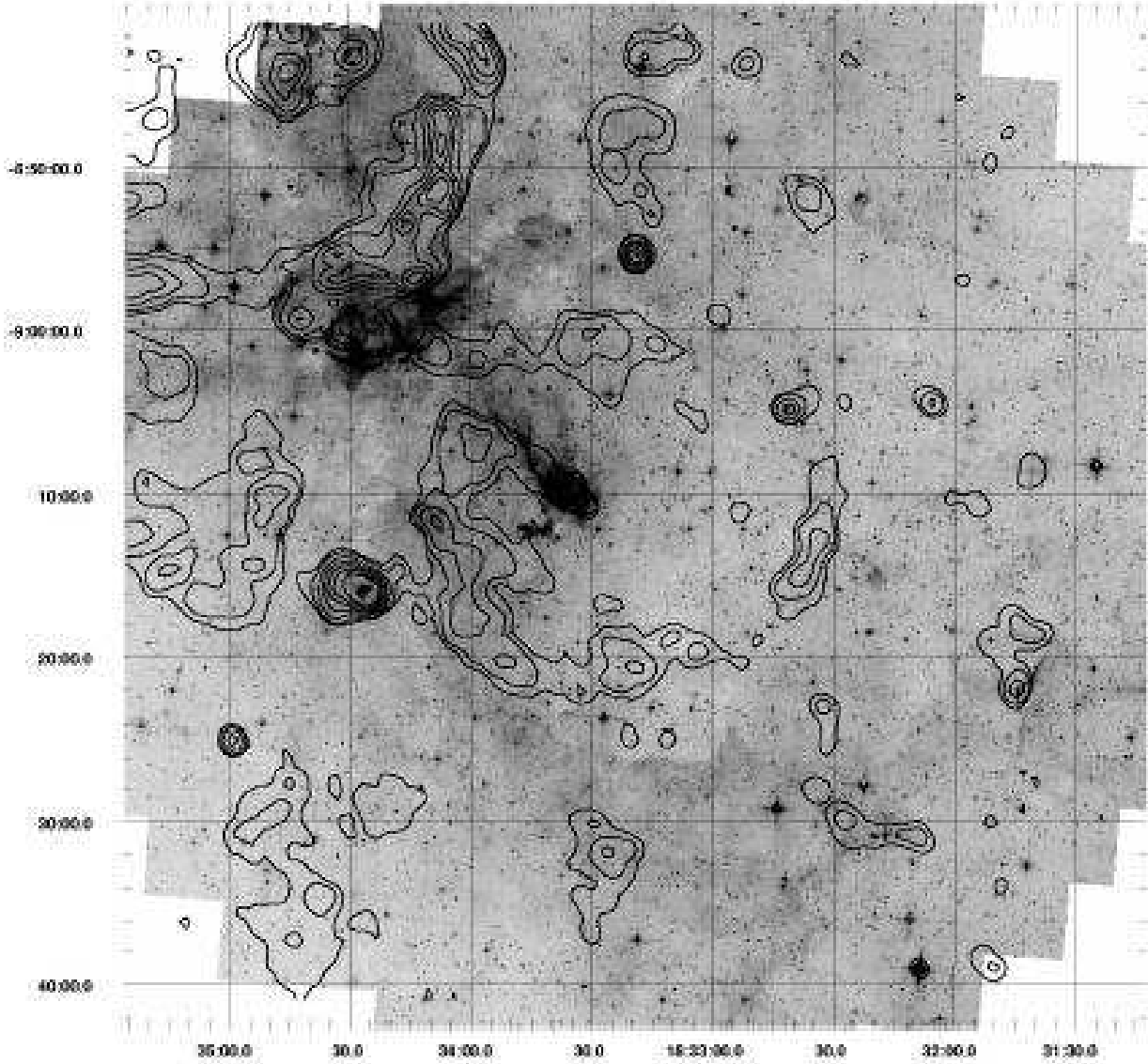


Fig. 6.— *Spitzer*/IRAC 5.8 μm image of the supernova remnant G22.7-0.2, with radio contours from the NVSS. W 41 is in the upper-left corner of this image. *NOTE: this figure was degraded in quality for distribution on astro-ph.*

W 41 (G23.3-0.3)—This SNR is located in an incredibly rich field of infrared emission, with a large H II region and embedded cluster (183447.3-083256) in the northern shell, diffuse red emission throughout the entire region, a dark lane running roughly north-south through the entire SNR, numerous compact H II regions and small shells, and extremely-red sources which are probably protostars. Some of these objects may be related to the SNR progenitor’s cluster. No detailed association between specific infrared features and the SNR were noticed (but see discussion of G22.7-0.2 above).

3C 391 (G31.9+0.0)— Figure 7 shows the IRAC images of 3C 391. This remnant was previously observed in the mid- and far-infrared using ISO: molecular and ionic lines include H₂, OH, H₂O, CO, [O I], and [O III] (Reach et al. 2000, 1998) and near-infrared imaging reveals shocked H₂ and [Fe II] emission (Reach et al. 2002). In Figure 7a, two green (channel 2) patches are evident; they are located at the northern and southern terminus of the bright radio semi-circular radio shell. The southern one comprises the ‘broad-molecular-line’ (BML) region 3C 391:BML (18^h49^m23.1^s-00°57′38″), where bright near-infrared H₂ emission and broad mm-wave molecular lines were previously detected (Reach et al. 2002); it also includes one of the two 1720 MHz OH masers spots associated with 3C391 (Frail et al. 1996). The IRAC color ratios for 3C 391:BML are consistent with shocked molecular gas. The northern patch (18^h49^m28.8^s-00°55′00″) also has associated near-infrared H₂ emission in a test image taken at Palomar (Reach et al. 2005); reanalysis of the CO and CS spectra reveals no broad molecular lines at this position. In addition to these patches, fainter and more extensive emission is evident in channels 2, 3, and 4, extending around the horseshoe-shaped radio shell.

The northwestern bar, where the brightest part of the radio shell is tangent to a giant molecular cloud, is detected in IRAC channels 2, 3, and 4 and is particularly bright in channel 3. This bar has very bright near-infrared 1.64 μm [Fe II] emission (Reach et al. 2002), and IRAC channel 3 contains the 5.34 μm line of [Fe II], whose upper energy level is the same as the lower energy level of the 1.64 μm; the 5.34 μm transitions should have at least comparable flux (and potentially much higher if the gas is cooler than 5000 K). If we interpret the IRAC channel 3 emission from the bar as entirely the 5.34 μm line, its surface brightness is 2×10^{-3} erg cm⁻² s⁻¹ sr⁻¹, while the 1.644 μm line brightness at the same position is 1×10^{-4} erg cm⁻² s⁻¹ sr⁻¹; this line ratio can be reproduced if the shocked gas has $T \sim 2200$ K (for $n \sim 10^2$ cm⁻³), which is entirely plausible for the fast J-shocks inferred for this location. Thus for the bright northwestern bar, IRAC channel 3 is likely to be [Fe II] line emission. Some contribution from Ar would be expected from such shocks in IRAC channel 4: the ISO 12–18 μm image was interpreted as a sum of [Ne II] and [Ne III] lines, and the situation should be similar for IRAC channel 4 containing [Ar II] and [Ar III]. Comparing the ISOCAM 12–18 μm and IRAC channel 4 image, the inferred ratio

$([\text{Ne II}] + [\text{Ne III}])/([\text{Ar II}] + [\text{Ar III}]) \sim 2$, which again is plausibly explained by gas behind a fast J-shock, with cosmic abundances Reach et al. (2002).

Thus for 3C 391, we find significant infrared emission correlated with the radio shell but with distinct colors: the ‘green’ (enhanced channel 2) regions are associated with near-infrared emission from H_2 and originate from shocked molecular gas, while the ‘magenta-red’ regions (enhanced channel 3) have associated near-infrared $[\text{Fe II}]$ and originate from shocked, ionized gas.

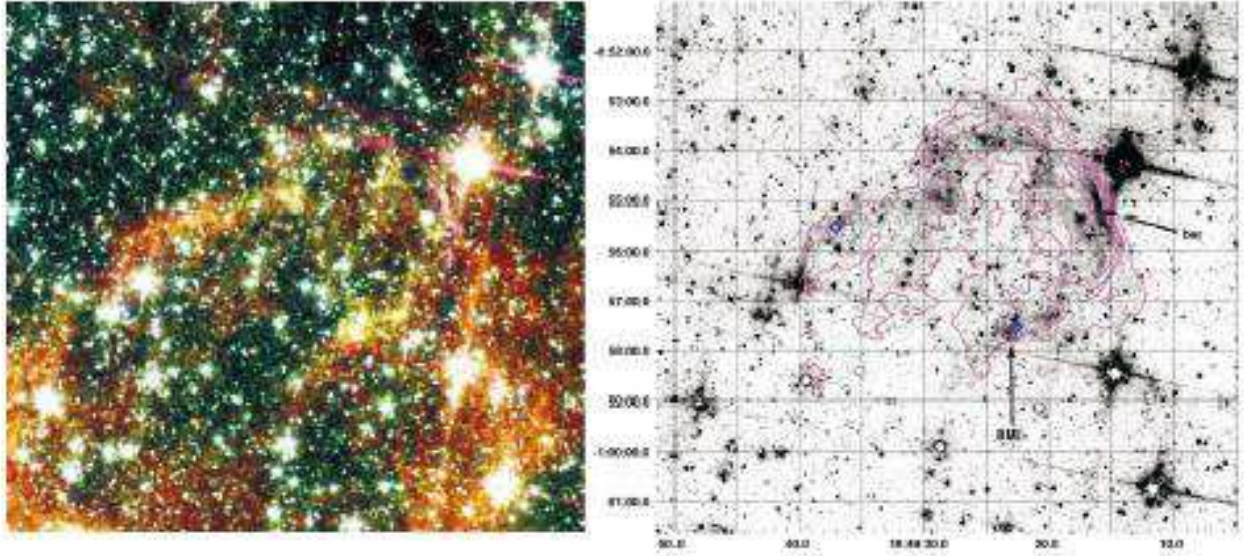


Fig. 7.— (a) *Spitzer*/IRAC color image of the supernova remnant 3C 391. The colors are red= $8\mu\text{m}$, green= $4.5\mu\text{m}$, blue= $3.6\mu\text{m}$, magenta= $I(5.8\mu\text{m}) - 0.308 \times I(8.0\mu\text{m})$. (b) *Spitzer*/IRAC $5.8\mu\text{m}$ image minus a scaled $8\mu\text{m}$ image to suppress emission with colors of normal interstellar medium. The radio contours (magenta) were constructed from VLA 20-cm data at $16''$ resolution (Brogan et al. 2005). The two OH masers are indicated with blue diamonds, and two features discussed in the text—the broad molecular line (BML) region and the radio bar—are labeled. *NOTE: this figure was degraded in quality for distribution on astro-ph.*

Kes 79 (G33.6+0.1)—Kes 79 was cataloged as a possible mixed-morphology SNR with centrally-filled X-rays detected by the ROSAT PSPC surrounded by a well-defined radio shell (Rho & Petre 1998). There is extensive mid-infrared emission near this SNR, with some features possibly at the distance of the remnant but no clear evidence for emission from shock fronts. Interestingly, there is an infrared dark cloud located near the eastern boundary of the SNR where CO observations suggest interaction with molecular clouds, although broad molecular lines were not detected (Green & Dewdney 1992). There are a number of point sources within the dark clouds with infrared colors consistent with those of protostars, and there are also a number of small diffuse structures similar to ultra-compact HIII regions. No infrared point source coincides with the compact central object (Seward et al. 2003).

W 44 (G34.7-0.4)—W44 is a mixed-morphology SNR featuring centrally-filled, thermal X-ray emission surrounded by a well-defined radio shell (Rho et al. 1994). The detections of broad molecular lines and shocked H₂ emission (Reach et al. 2005 and references therein) unambiguously show that the remnant is interacting with molecular clouds. The *Spitzer* color image of W44 in Figure 8 is one of the best images from this survey. A large, green, elliptical shell matches the radio shell rather closely. In particular, the IRAC channel 2 image emission is almost identical to the near-infrared H₂ images taken for the fields towards the northeastern and southern portions of the shell (Reach et al. 2005), indicating that this emission is from shocked H₂. This is also consistent with the line contribution we estimated based on the color ratio of the four channel described in §2 and validates our predicted IRAC colors for molecular shocks. There is an infrared-dark cloud at the boundary of the eastern shell of W44. The patch of red emission south of the dark cloud is likely a small H II region based on the ratio of H α and [S II] (Rho et al. 1994). The IRAC channel 3 image is similar to the channel 2 image, as expected because bright H₂ lines in channel 2 will always be accompanied by bright lines in channel 3. But channel 3 is mixed with the eastern H II region and other ISM emission outside the remnant. The remnant is barely noticeable in IRAC channel 4 due to confusion with unrelated emission.

G36.6-0.7—There is a possible shell of infrared emission bounding the SNR toward the North, as well as a dark filament in the N and clumps in the W and SW. There is no clear evidence for emission from shock fronts.

3C 396 (G39.2-0.3)—Infrared emission is detected from this remnant in three forms. First, faint, filamentary emission is detected in the western radio shell of this remnant, with IRAC colors clearly distinct from normal interstellar emission. In Figure 9a, the western shell appears green; a cut through the western shell near $19^{\text{h}}03^{\text{m}}56.3^{\text{s}}+05^{\circ}25'46''$ yields IRAC colors (< 0.08)/0.2/0.69/1, suggesting emission from shocked, ionized gas.

Second, there are two very bright infrared filaments, at $19^{\text{h}}04^{\text{m}}18.5^{\text{s}}+05^{\circ}20'33''$ and $19^{\text{h}}04^{\text{m}}17.0^{\text{s}}+05^{\circ}27'07''$ (each $\sim 30''$ long) just inside the eastern radio shell. The filaments are clearly separated from the recently-detected pulsar wind nebula (Olbert et al. 2003) and are located within a region of exceptionally high radio polarization. We suspect these bright filaments, which are highly unusual, are part of the supernova remnant, which is the only known structure in the interstellar medium at that location. The color ratios of the filaments are $(< 0.05)/0.03/0.4/1$, at a location where the $8 \mu\text{m}$ surface brightness is 30 MJy sr^{-1} . These colors are similar to normal interstellar medium, so the filaments could be photodissociation regions (e.g. compressed filaments that were shocked long ago, rather than active shock fronts).

Finally, there is faint, diffuse emission surrounding the entire radio shell, with some bright, extended regions just outside the eastern periphery. The ‘blowout tail’ discussed by Patnaik et al. (1990) from radio data extends eastward from the remnant and wraps north then back over the top of the remnant. In the infrared, the ‘tail’ starts with a bright region at $19^{\text{h}}04^{\text{m}}26.0^{\text{s}}+05^{\circ}27'55''$ that is connected to an intricate set of infrared filaments that follow the radio structure, with the infrared region displaced somewhat southward. While this ‘tail’ could be an H II region, the remarkably high radio polarization (50%) suggests most of the radio emission is synchrotron radiation. Thus the ‘tail’ could be due to energetic particles in a plume extending through ‘hole’ in the eastern shell of the remnant. The bright infrared region near the base of the ‘tail’ is detected only in channels 3 and 4, with a ratio 0.3:1 consistent with photodissociation regions or H II regions.



Fig. 8.— *Spitzer*/IRAC color image of W 44. The SNR appears ‘green’ in the IRAC colors because channel 2 is relatively much brighter in the SNR shell than in the surrounding ISM (including both the surrounding molecular cloud and the H II regions to the E and NE). *NOTE: this figure was degraded in quality for distribution on astro-ph.*

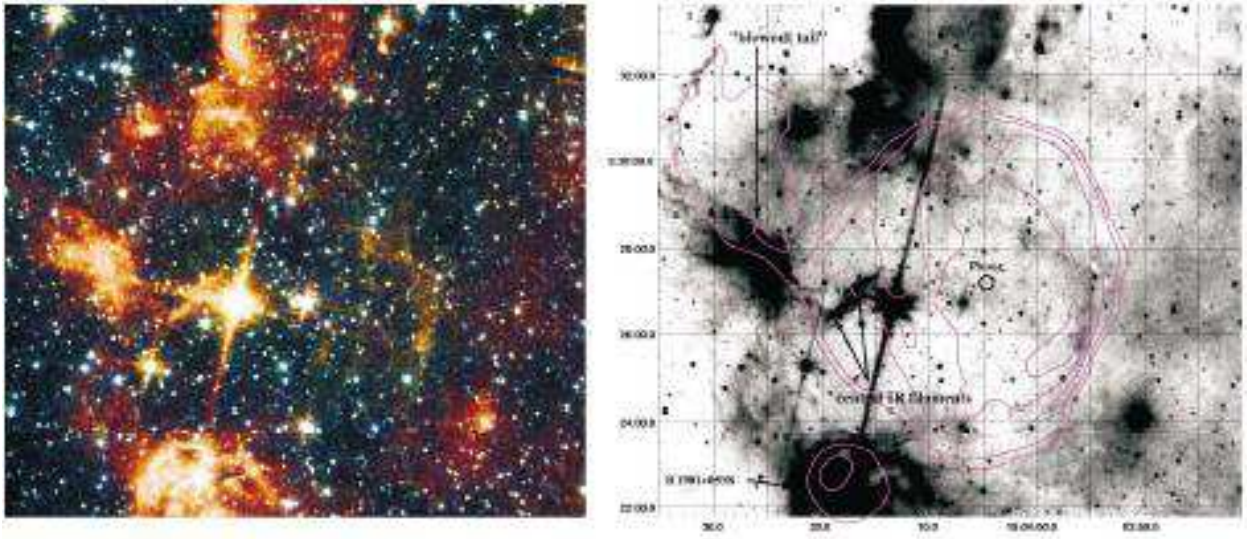


Fig. 9.— (a) *Spitzer*/IRAC color image of the supernova remnant 3C 396 (G39.2-0.3). The colors are red= $8\mu\text{m}$, yellow= $5.8\mu\text{m}$, green= $4.5\mu\text{m}$, blue= $3.6\mu\text{m}$. (b) *Spitzer*/IRAC $8\mu\text{m}$ image of the supernova remnant 3C 396 (G39.2-0.3), with radio contours overlaid. The infrared greyscale is logarithmic. The radio image was generated using 20-cm images from the VLA archive; contours levels are 1.5, 4.2, 12, 26, 45 mJy/beam (with $15''$ resolution). Features discussed in the text are labeled. *NOTE: this figure was degraded in quality for distribution on astro-ph.*

3C 397 (G41.1-0.3)—This small remnant has faint mid-infrared emission that clearly correlates with portions of the radio shell. Figure 10 shows relatively distinct filaments near $19^{\text{h}}07^{\text{m}}40.5^{\text{s}}+07^{\circ}08'48.''$ The infrared emission was detected in channel 2, 3, and 4, with ratios 0.1/0.8/1 (for channels 2/3/4) that are inconsistent with photodissociation regions and H II regions but are plausible for fine-structure lines from shocked gas. The high $5.8 \mu\text{m}$ brightness could be due to efficient grain destruction leading to a bright Fe II $5.3 \mu\text{m}$ line.

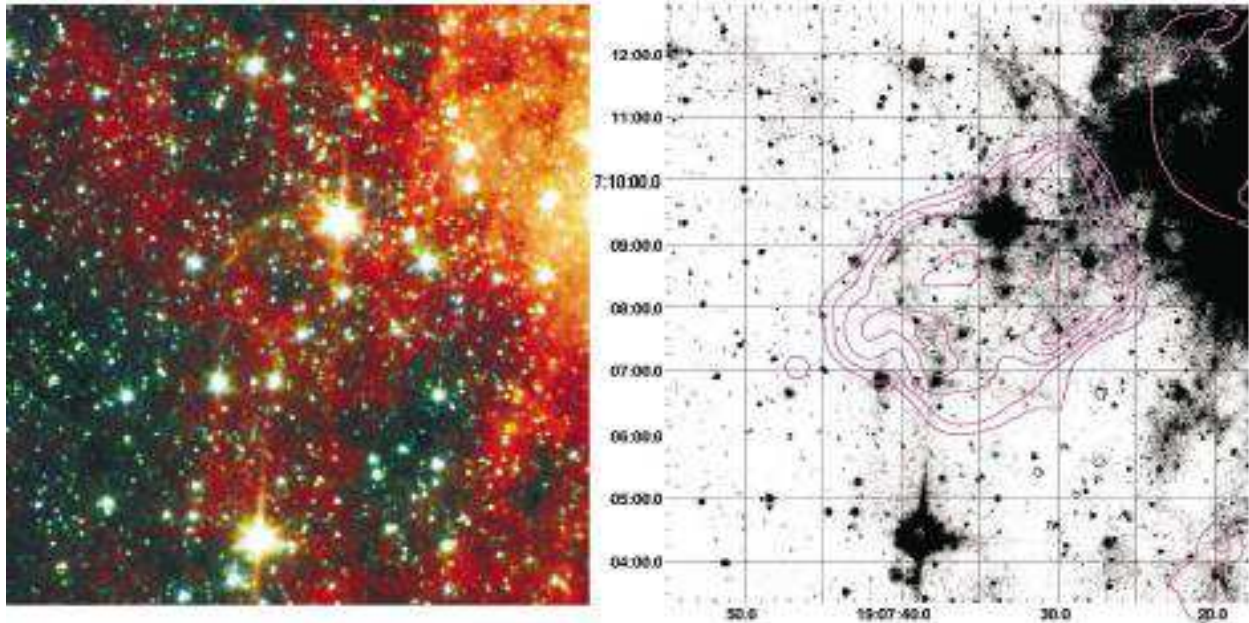


Fig. 10.— (a) *Spitzer*/IRAC color image and (b) $5.8 \mu\text{m}$ image of 3C 397 with radio contours overlaid. The infrared greyscale is logarithmic. The radio image was generated using 20-cm images from the VLA archive; contours levels are 10, 46, 83, 120 mJy/beam (with $\sim 15''$ resolution). *NOTE: this figure was degraded in quality for distribution on astro-ph.*

W 49B (G43.2-0.2)—W 49B has a relatively unique structure, with its radio emission forming a set of curved filaments in either a spiral or barrel-hoop morphology (Moffett & Reylonds 1994). The X-ray emission is thermal with rich line emission, mostly attributed to ejecta material, indicating it is a rather young SNR (Hwang et al. 2000). The SNR is clearly detected in the IRAC/GLIMPSE images. Figure 11 shows the IRAC color image, with the emission from the SNR clearly dominating over other nearby diffuse emission. There are two very distinct colors (green and magenta in Fig. 11). Much of the SNR has a filamentary structure, and this part of the IRAC image closely follows the radio morphology, with its series of loops. These appear relatively ‘magenta’ in Figure 11 due to very bright emission in channel 3. The color ratios toward a radio and near-

infrared [Fe II] filament near $19^{\text{h}}11^{\text{m}}07.0^{\text{s}}+09^{\circ}07'01''$ (Table 2) suggest line emission from ionic shocks. Another distinct component of the infrared emission, forming a sort of outer shell toward the east and southwest, appears relatively ‘green’ in Figure 11; the colors toward $19^{\text{h}}11^{\text{m}}14.3^{\text{s}}+09^{\circ}04'42''$ (Table 2) are consistent with lines from shocked molecular gas. The presence of these two distinct types of shock was first found in near-infrared, narrow-band images, which show [Fe II] $1.66 \mu\text{m}$ and radio emission distributed like the ‘magenta’ emission in Figure 11 and H_2 $2.12 \mu\text{m}$ emission distributed like the ‘green’ emission in Figure 11 (Keohane et al. 2005). This remnant, together with 3C 391, serve as an empirical validation of the IRAC color interpretations in this paper using near-infrared narrow-band imaging.



Fig. 11.— *Spitzer*/IRAC color image of the supernova remnant W 49B, with red= $8\ \mu\text{m}$, green= $4.5\ \mu\text{m}$, blue= $3.6\ \mu\text{m}$, and magenta= $5.8\ \mu\text{m}$ minus a scaled $8\ \mu\text{m}$ image. There are two distinct types of emitting region, the molecular emission is green and is brighter at the eastern and southwestern extremities, while the ionic emission is magenta and is brighter in the radio ‘loops.’ *NOTE: this figure was degraded in quality for distribution on astro-ph.*

G45.7-0.4—There is an infrared filament approximately parallel to part of the radio shell around $19^{\text{h}}16^{\text{m}}36.0^{\text{s}}+11^{\circ}08'00''$, and a potentially related arc near $19^{\text{h}}16^{\text{m}}30^{\text{s}}+11^{\circ}14'16''$, but no clear evidence for emission from shocked gas or dust.

G54.4-0.3—The cluster containing the progenitor of this SNR blew a large stellar wind bubble, into which shocks are now propagating. A shell of molecular gas was found to be surrounding the SNR, containing protostar candidates (Junkes et al. 1992). Figure 12 shows two regions where infrared filaments follow the radio shell. The features are located along the nonthermal, western hemisphere of the radio shell evident at low frequencies (Velusamy, Goss & Arnam 1986). These are likely the locations of shocks into the wind-blown bubble and/or molecular cloud. The western filament is centered on $19^{\text{h}}32^{\text{m}}07.7^{\text{s}}+19^{\circ}02'56''$, and the northern filament is centered on $19^{\text{h}}33^{\text{m}}12.6^{\text{s}}+19^{\circ}16'20''$. The colors of the filaments are similar to photodissociation regions, so it is not certain whether the emission is due to shocks. However, there is an infrared shell in both the 5.8 and 8 μm images, approximately following much of the radio shell. Bright H II regions are located within the shell, with some of them (e.g. G54.38-0.05) possibly connecting with shell filaments. These could be a generation of stars that has formed in the shell surrounding the progenitor of the SNR (Junkes et al. 1992).

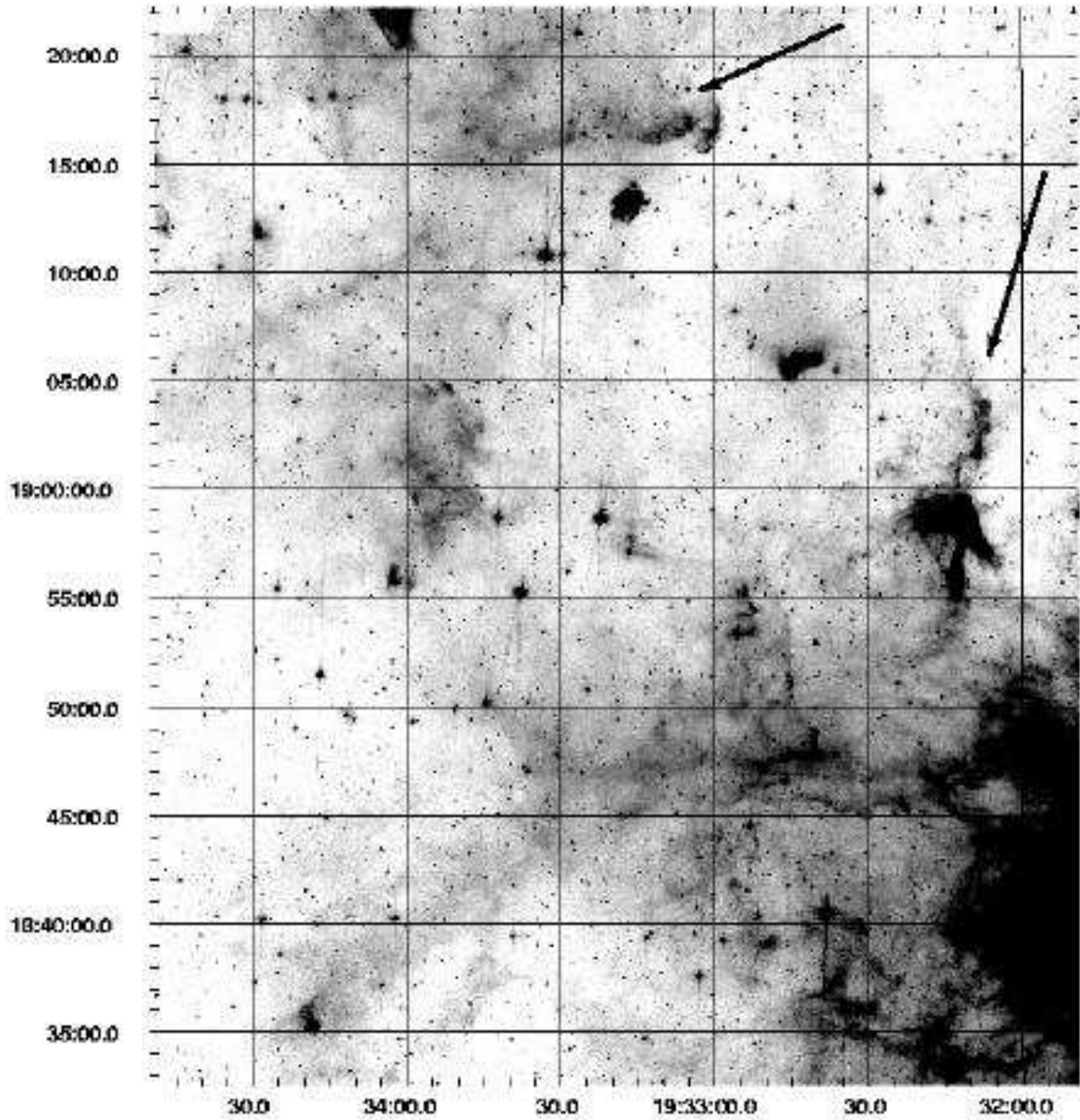


Fig. 12.— *Spitzer*/IRAC 8 μ m image of the supernova remnant G54.4-0.3. The two filaments discussed in the text are marked with arrows. *NOTE: this figure was degraded in quality for distribution on astro-ph.*

G55.0+0.3—A large diffuse arc (3' wide) possibly relates to the eastern radio shell, but the association is not clear.

Kes 17 (G304.6+0.1)— Kes 17 is a relatively unstudied SNR. The *Spitzer*/IRAC images reveal bright mid-infrared emission shown in in Figure 13. The images show bright channel 2 emission (green in Fig. 13 and likely due to shocked H₂) in the NW rim. Detailed arc structures are noticeable in the images, and the remnant is bright in all IRAC channels. The IRAC colors of the pair of the thin isolated filament near 13^h05^m46.2^s-62°38'33" are somewhat more extreme (brighter in channels 1 and 3, relative to channel 4) than those toward the brightest part of shell (see Table 2). Based on the colors and the detailed morphological agreement of the images in all 4 channels—channel 1 in particular is not expected from ionic shocks—most of the mid-infrared emission from the shell could be from molecular shocks. The radio continuum emission shows clear shells in the northwest and south. Infrared dark clouds and globules are present north of Kes 17 (13^h06^m33.5^s-62°34'00.3)" which includes green sources (possible protostars) and possible compact H II regions. It is not known whether this star forming region is associated with (or even at the same distance as) Kes 17.

G308.8-0.1—This large remnant comprises a very bright northern bar (G308.7+0.0) with a southward projection, and a southern arc (G308.9-0.2). Interpreted as a single SNR, the diameter is 25', contains the pulsar J1341-6220, and is located at ~ 7 kpc, behind most of the bright H II regions in the field (Caswell et al. 1992). The IRAC images contain a wealth of emission; the brightest emission is obviously associated with the brightest H II regions. Two features are of interest with regard to the SNR. First, following the entire extent of the northern bar, there is a dark cloud. In fact, the northern bar seems to nestle within a void of infrared emission. Within the dark cloud, there are three embedded sources: 13^h40^m20.7^s-62°16'34" (very red point source, probable massive protostar), 13^h40^m57.0^s-62°13'05" and 13^h32^m03.0^s-62°11'41" (two bright red blobs probably containing young B stars). It is hard to say whether or how this dark cloud and its embedded sources are related to the remnant, particularly if the remnant is relatively distant. The second relevant infrared feature is extensive filamentary emission within the southern arc (G308.9-0.2). A remarkable set of bright filaments is near 13^h42^m08.5^s-62°32'45;" the IRAC colors of these filaments are 0.02/0.02/0.36/1, similar to normal, unshocked interstellar PAH. The 5.8 μ m image seems to form a shell including the southern arc and with a northern boundary far to the south of G308.7+0.0. Based only on the radio and infrared emission, we might conclude that there are two separate remnants. However, any infrared emission from the northern portion of the SNR is actually extinguished by the dark cloud that is seen in projection against G308.7+0.0 (regardless whether or not the dark cloud and G308.7+0.0 are associated).



Fig. 13.— *Spitzer*/IRAC color image of the supernova remnant Kes 17. The image is in equatorial coordinates and has size $13' \times 11'$. *NOTE: this figure was degraded in quality for distribution on astro-ph.*

Kes 20B (G310.6-0.3)—Very dark clouds surround this remnant, including remarkable large clouds completely opaque at $8\ \mu\text{m}$ to the N and E. While the present data do not clearly reveal an interaction with these clouds, an interaction may be occurring to the N where the radio contours run along the long axis of a dark cloud. Some $8\ \mu\text{m}$ emission appears around the border of the remnant but does not have a detailed relationship to the radio contours and could be unrelated. A notable feature occurs inside the remnant, approximately along a faint inner radio ridge. It is a thin filament, centered on $13^{\text{h}}58^{\text{m}}08^{\text{s}}-62^{\circ}07'03''$, with position angle 67° E of N and length $23''$, and it has IRAC colors consistent with a molecular shock. Without a higher-resolution radio image (to correlate with the infrared filament), or a more-sensitive infrared image (to find other such features) it is not possible to tell whether this is a shock front into a molecular cloud or a massive molecular outflow from a young stellar object. There is no obvious young stellar object in the IRAC images. Based on the present data we can only suggest some infrared emission *may* be related to the remnant, but there is not enough evidence to call this remnant a detection.

Kes 20A (G310.8-0.4)—This large remnant (Figure 14) has a distinctive radio morphology defined by a very bright ridge running roughly north-south, defining what could be the eastern hemisphere of a shell; the western hemisphere is not clear in the nonthermal radio image. Extensive infrared emission approximately follows the radio ridge. The infrared emission breaks into many narrow clumps and arcs. Based on the infrared image alone, these would appear to be small H II regions or reflection nebulae. Indeed numerous similar features that exist throughout the region are clearly unrelated to Kes 20A. The brightest such H II regions are evident in the MOST radio image as individual sources, clearly distinct from the nonthermal ridge that defines the remnant. In addition to the emission along the eastern ridge, similar filamentary infrared emission occupies part of what would be the interior of the remnant, based on the incomplete-shell radio morphology. Additional, similar infrared emission is located outside the remnant and clearly not directly related. The high density of H II regions and proximity to the SNR Kes 20B show this region to be rife with massive stars. Thus the emission that appears plausibly associated with Kes 20A could be a chance association or a second-generation association due to younger stars that formed in a wind-blown bubble generated by the progenitor. A slice through the SE portion of the remnant yields infrared colors $0.13/0.13/0.67/1$ that do not match the color templates described above very well but are generally similar to those of photodissociation regions, which supports a second-generation (as opposed to shock-powered) origin for the present infrared emission.

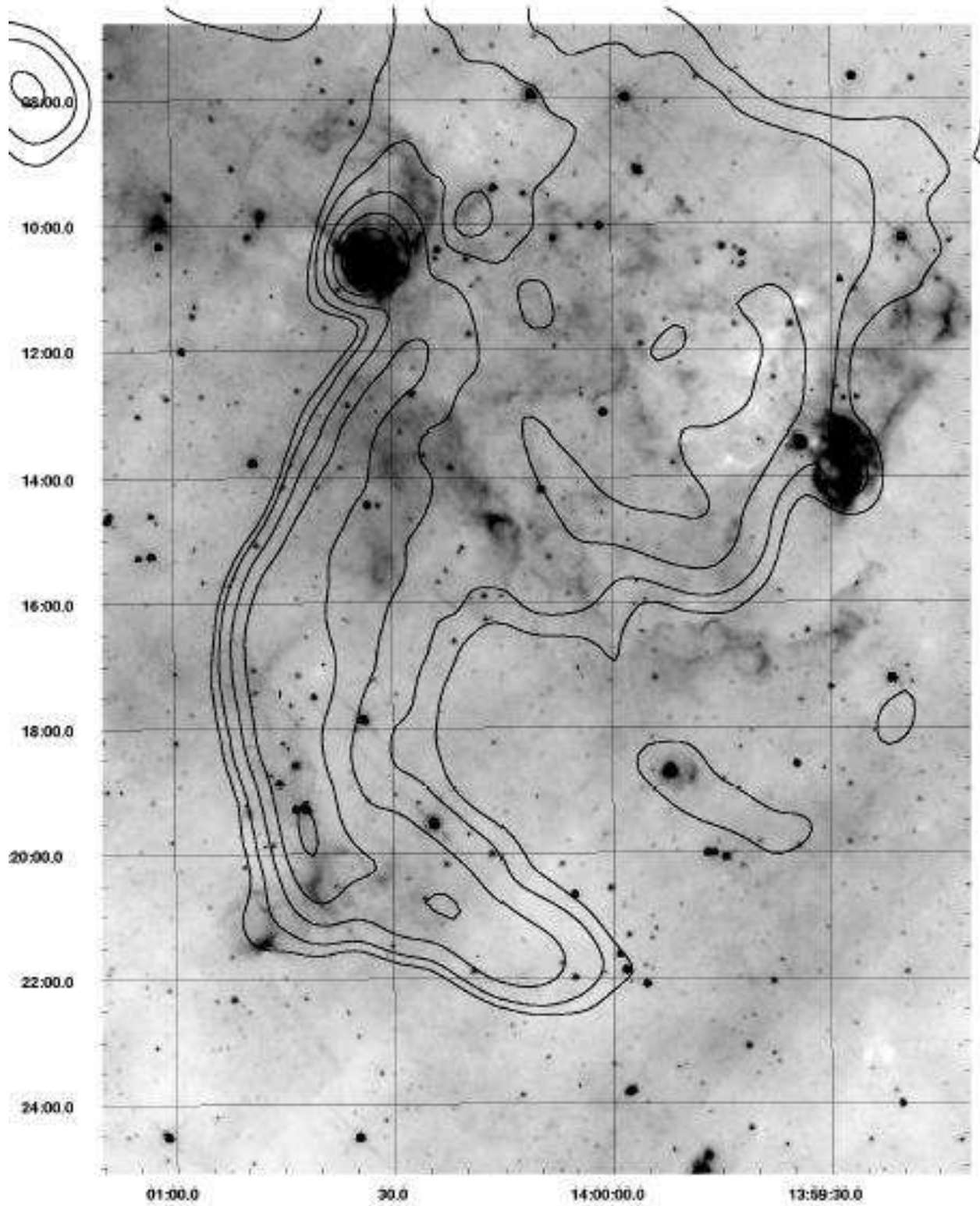


Fig. 14.— *Spitzer*/IRAC image of the supernova remnant Kes 20A, with radio continuum contours from the MSC overlaid. *NOTE: this figure was degraded in quality for distribution on astro-ph.*

G311.5-0.3—This shell-type remnant is one of the most easily detected in the present survey, because it so clearly follows the entire radio shell and it is in a relatively uncluttered region. Cohen and Green (2001) compared MOST observations with $8.3 \mu\text{m}$ observations made with the Midcourse Space Experiment (MSX) and reported no detection. Figure 15 shows the Spitzer/IRAC image, which is significantly deeper than MSX, so the SNR is evident in all 4 channels. The IRAC images show a nearly complete shell of infrared emission corresponding well with the radio shell. Bright narrow filaments line the western edge of the SNR, with two bright ridges giving a ‘braided’ appearance over a significant portion of the western shell. The infrared shell is particular bright near $14^{\text{h}}05^{\text{m}}21.9^{\text{s}}-61^{\circ}58'06''$ and a less-confused filament nearby ($14^{\text{h}}05^{\text{m}}22.6^{\text{s}}-61^{\circ}57'22''$) has IRAC color ratios 0.3/0.4/1/1 suggesting the IRAC emission is from shocked gas. Two bright, red, compact sources at $14^{\text{h}}05^{\text{m}}24.3^{\text{s}}-61^{\circ}57'07''$ and $14^{\text{h}}05^{\text{m}}23.5^{\text{s}}-61^{\circ}56'58''$ are possibly Class 0 protostars located just at the edge of the SNR.

Kes 27 (G327.4+0.4)— The mid-infrared image shows a set of bright filaments with diffuse emission centered on a radio peak within the remnant near J154912-534420 (G327.39+0.47). Figure 16 shows the correspondence between this region and the radio shell. This filamentary source could be the location of shocks into a dense cloud, possibly containing an embedded massive star, so we consider it in more detail. The MOST 843 MHz image (Whiteoak & Green 1996) shows a resolved but simple (centrally condensed) peak with a FWHM of $2.2'$ and a flux of approximately 0.4 Jy (from aperture photometry centered on the source with annular background removal). The Parkes 5 GHz image (Milne & Dickel 1975) does not show a corresponding structure, at least partially due to its low angular resolution ($4.4'$). If the source is an H II region with thermal spectrum, the flux at 5 GHz would be ~ 0.2 Jy and the brightness temperature ~ 0.3 K after diluting to the Parkes 5 GHz beam. On the other hand, if the source is nonthermal with spectral index 0.7, then the brightness temperature at 5 GHz would be 0.06 K. There is no structure in the 5 GHz image above 0.2 K, which is consistent with nonthermal emission and marginally inconsistent with thermal emission. McClure-Griffiths et al. (2001) show a 1420 MHz continuum image of the remnant (their Fig. 13). The radio peak corresponding to the infrared region is evident in their image, with a flux of approximately 0.2 Jy (counting contours). The 1420 MHz and 843 MHz contour maps are nearly identical after a linear transformation, indicating that the infrared filamentary source has about the same spectral index as the rest of the remnant emission. Improved radio continuum observations are needed to assess the nature of the source. The mid-infrared colors of this region are more typical of PAH-dominated photo-dissociation regions than shocked gas. McClure-Griffiths et al. (2001) show from 21-cm line observations that there is an H I ridge just outside the southwestern radio contours. There are no obvious protostar candidates in the region, so the impact has evidently not

triggered star formation; this is not surprising given the remnant is thought to be relatively young, with estimates of 2400 yr (McClure-Griffiths et al. 2001) and 3500 yr (Seward et al. 1996) [cf. $> 8 \times 10^4$ yr (Enoguchi et al. 2002)]. The true nature of this region awaits future investigation.

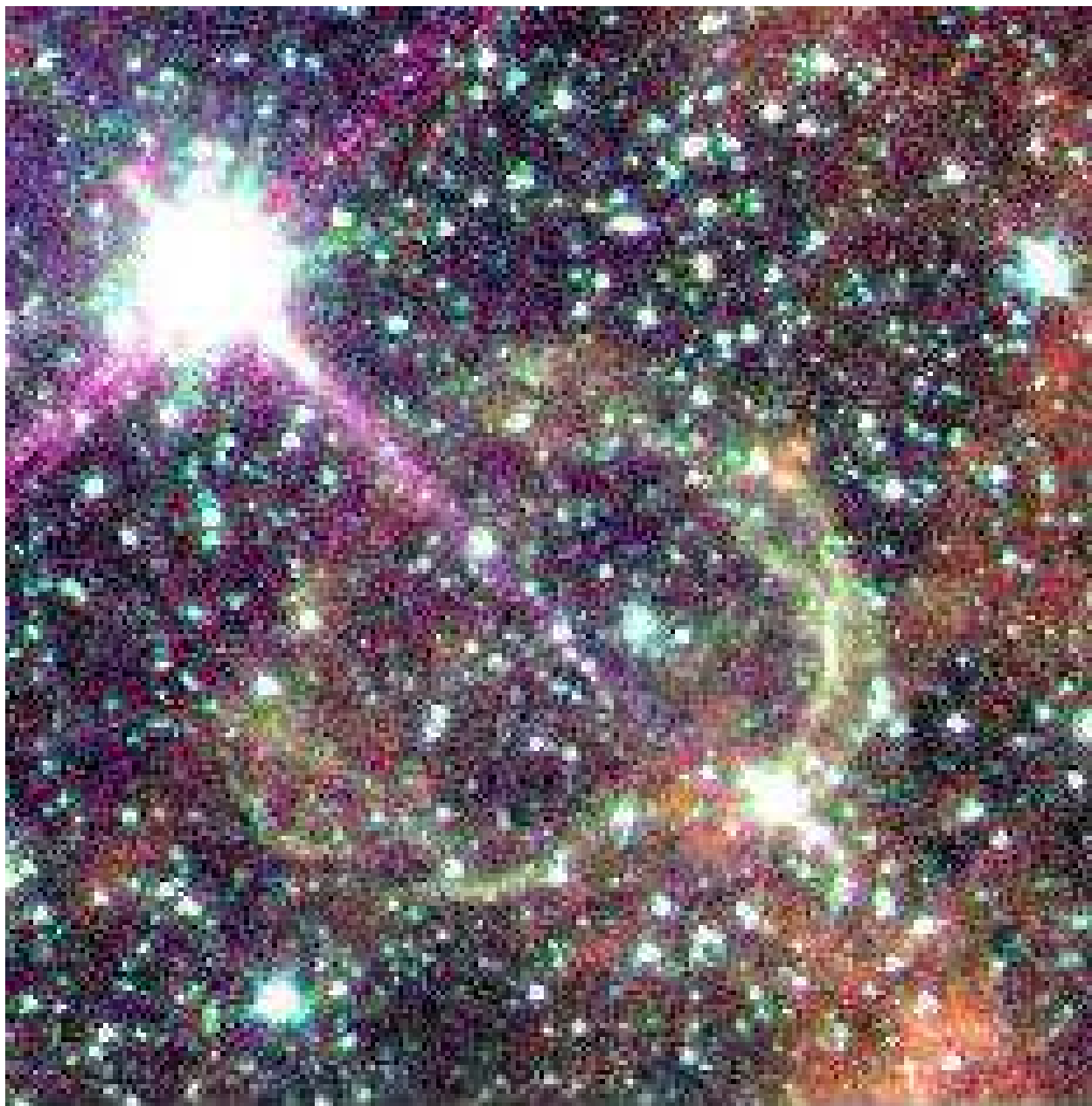


Fig. 15.— *Spitzer/IRAC* color image of the supernova remnant G311.5-0.3, with red= $8\ \mu\text{m}$, green= $4.5\ \mu\text{m}$, blue= $3.6\ \mu\text{m}$, and magenta= $5.8\ \mu\text{m}$ minus a scaled $8\ \mu\text{m}$ image. The entire shell of the SNR is evident, with a double-stranded morphology. *NOTE: this figure was degraded in quality for distribution on astro-ph.*

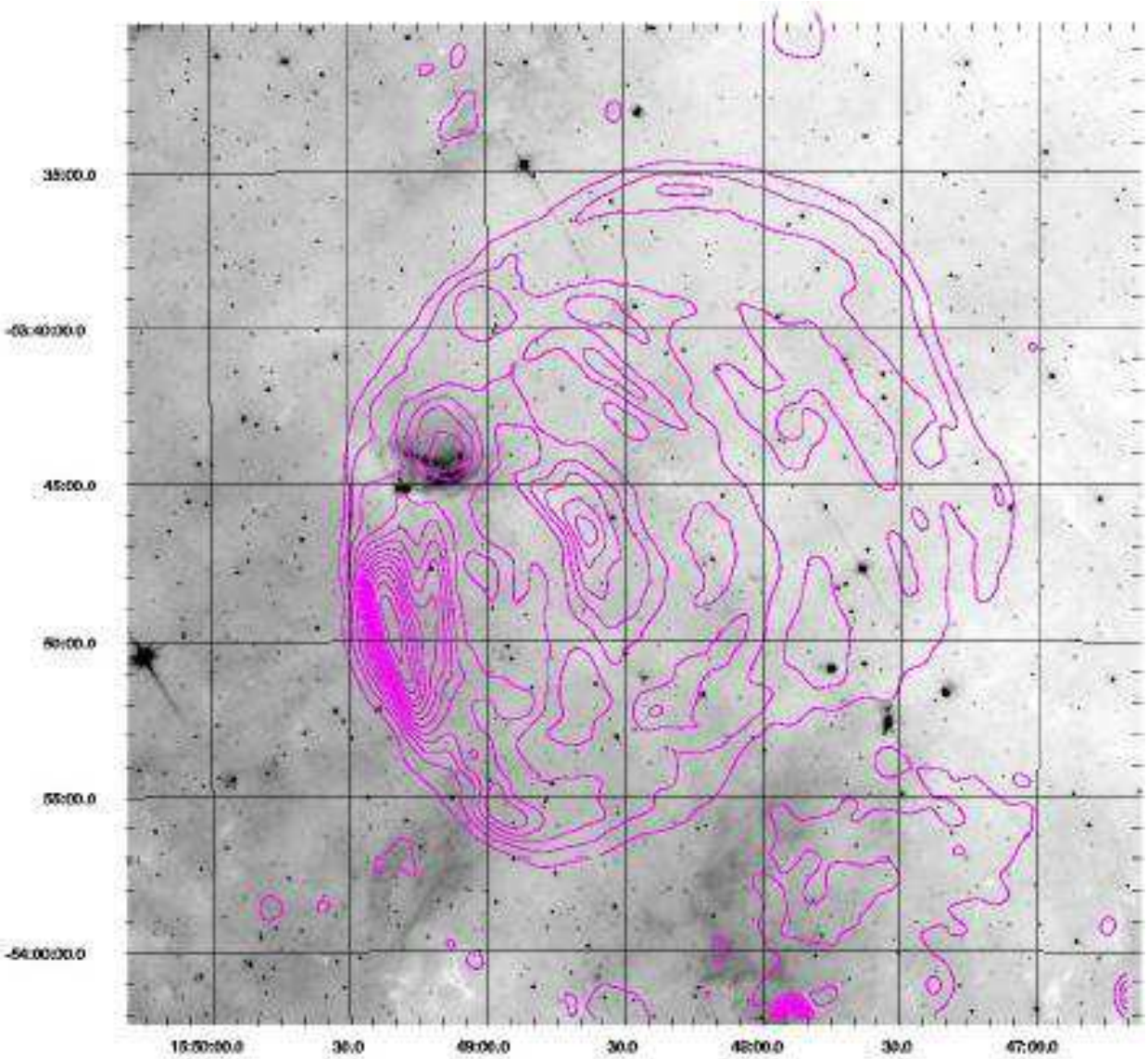


Fig. 16.— *Spitzer*/IRAC 8 μm image of the supernova remnant Kes 27, with radio contours from the NVSS overlaid. *NOTE: this figure was degraded in quality for distribution on astro-ph.*

G329.7+0.4—The SW corner of this remnant has bright extended mid-infrared emission that follows some of the radio structures, in particular the SW corner of the remnant and a bright spur penetrating into the remnant from $16^{\text{h}}00^{\text{m}}39.9^{\text{s}}-52^{\circ}30'46''$ to $16^{\text{h}}01^{\text{m}}10.3^{\text{s}}-52^{\circ}25'24''$ (and beyond). The corner and spur have similar brightness to some H II regions, but their orientation along a radio filament that appears to be part of the remnant makes them plausibly part of the remnant. On the other hand there are some mid-infrared spurs that appear related to this same region but directed well outside the remnant. The colors of the bright bar are 0.03/0.02/0.33/1 (toward a location where the $8\ \mu\text{m}$ surface brightness is $66\ \text{MJy sr}^{-1}$) look like PAH emission or an H II region. A ‘shell’ of mid-infrared shell surrounds the remnant on the eastern and southern sides, connecting to the bright SW corner and the western side of the remnant. This ‘shell’ breaks into some moderately bright patches that may be individual H II regions or photodissociation regions from B stars. The overall box-like shape of the region is very similar to the outer boundary of the nonthermal emission from the supernova remnant. Therefore, we suspect that it is in fact related to the remnant, even though it is unlikely to be emission from shocked dust and gas. Instead it probably represents a fossil shell, due to the stellar winds and supernovae of the previous generation of massive stars, into which the present remnant is now expanding. A relatively diffuse part of the shell has colors 0.05/0.04/0.6/1 (toward a location where the $8\ \mu\text{m}$ surface brightness is $11\ \text{MJy sr}^{-1}$), most similar to PAH regions or H II regions.

RCW 103 (G332.4-0.4)— The IRAC images (Figure 17) in all 4 channels show relatively bright, diffuse emission associated with the SNR RCW 103. In particular channel 2 shows strong emission at the southern shell and faint emission in the northwest and western shell. H_2 , [Fe II] and [Ar II] lines were previously detected in ISO spectra, and the emission was spatially resolved in the ISOCAM FOV 1/5 image (Oliva et al. 1999). Therefore, we measure the IRAC color from two positions of the SNR. A slice through the filament near $16^{\text{h}}17^{\text{m}}32.8^{\text{s}}-51^{\circ}06'28''$ yields colors 0.14/0.28/0.86/1 (with $8\ \mu\text{m}$ brightness $14.5\ \text{MJy sr}^{-1}$), most likely dominated by shocked molecules (but with some ionic contribution in channel 3). Much of the southern rim has such colors. A thin filament near $16^{\text{h}}17^{\text{m}}45.7^{\text{s}}-51^{\circ}04'58''$ (Table 2) is undetected in channel 1 despite being very distinct in channel 3 indicating ionic shocks. The two types of emitting regions can be discerned in Figure 17, with the primarily-molecular shocks appearing green and the primarily-ionic shocks appearing magenta. There are a number of H II regions and dark clouds surrounding RCW 103.

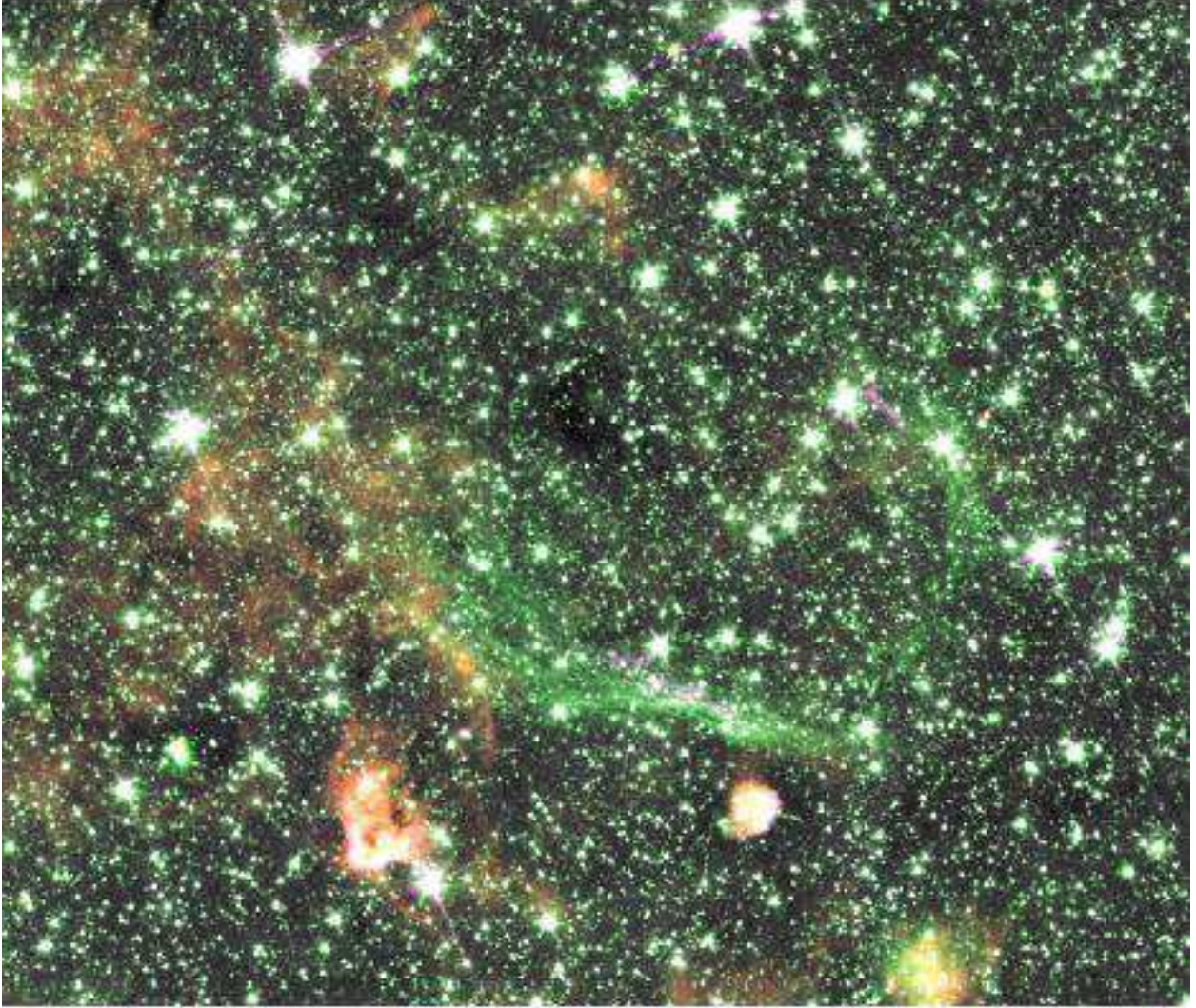


Fig. 17.— *Spitzer*/IRAC color image of the supernova remnant RCW 103, with red= $8\ \mu\text{m}$, green= $4.5\ \mu\text{m}$, blue= $3.6\ \mu\text{m}$, and magenta= $5.8\ \mu\text{m}$ minus a scaled $8\ \mu\text{m}$ image. The SNR is most clearly separated from the diffuse galactic emission by its $4.5\ \mu\text{m}$ emission, but it is detected in all 4 IRAC channels. There are at least two distinct emitting regions; the dominant one (seen in all 4 channels) is green in this rendition, while a fainter one (most noticeable at $5.8\ \mu\text{m}$) is magenta in this rendition. *NOTE: this figure was degraded in quality for distribution on astro-ph.*

Kes 32 (G332.4+0.1)—There is no mid-infrared emission corresponding to the radio contours from MOST. However, there is a very bright infrared H II region in the southwestern part of the remnant. The H II region is centered near $16^{\text{h}}15^{\text{m}}37.9^{\text{s}}-50^{\circ}44'06''$ and has a central cavity containing what appears to be a cluster of young stars. Protrusions extend from this H II region in many directions, including narrow filaments and what appears to be a very large ‘plume’ extending to the northwest of the H II region, directly across the western half of Kes 32. It is not clear which features are associated with the remnant and which are associated with the H II region. However, the high-resolution Spitzer/IRAC image shows the ‘plume’ connects directly to the H II region and is most likely associated with it. This contradicts an earlier conjecture that the plume, which can be seen in radio images, could be a jet of energetic particles from the stellar remnant of Kes 32 (Roger et al. 1985). Instead, we suspect that the plume originates from the H II region and is being ionized by the current generation of young stars within it.

G344.7-0.1—G344.7-0.1 has not been well studied, but the radio morphology is shell-like with a bright northwestern shell (Dubner et al. 1993). Figure 18 reveals an area of irregularly-structured infrared emission about $2'$ in diameter near $17^{\text{h}}03^{\text{m}}55.1^{\text{s}}-41^{\circ}40'43''$. The colors (Table 2) suggest the emission is likely due to shocked ionized gas. Figure 18 shows the mid-infrared emission coinciding with the central radio peak from the MOST supernova remnant catalogue (Whiteoak & Green 1996). This is the first detection in the infrared; it was not seen in previous IRAS surveys (Arendt 1989; Saken, Fesen, & Shull 1992).

G346.6-0.2—The SNR is surrounded in the N and W by diffuse infrared emission ($5.8\text{--}8\ \mu\text{m}$). The emission associated with the remnant is a narrow rim that follows the southern radio shell. The IRAC colors of the rim are very distinct, so the rim is evident in the color image (Figure 19a). This southern rim more-or-less connects the three OH 1720 MHz masers associated with the remnant. The IRAC colors suggest molecular shocks, consistent with their close association with the OH masers. In addition to the southern rim, there is possibly some infrared emission following the northern shell, but it is not readily evident in the Figures.

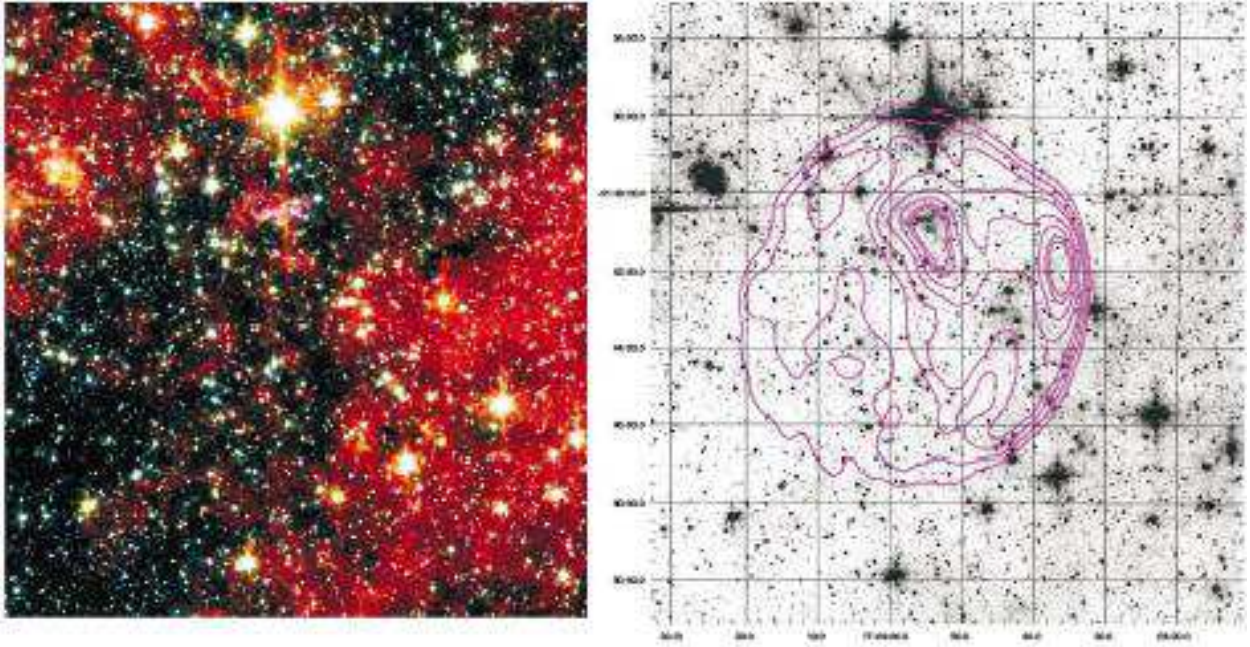


Fig. 18.— (left) *Spitzer*/IRAC color image of G344.7-0.1, with red=channel 4, orange=channel 3, green=channel 2, blue=channel 1, and magenta=channel 3 minus $0.3 \times$ channel 4. The filament associated with the N radio peak in the SNR is relatively bright in channel 3 and appears ‘magenta’ in this image. (right) *Spitzer*/IRAC channel 3 image of G344.7-0.1, with radio contours from the MSC overlaid. The greyscale ranges from 15 to 30 MJy sr⁻¹. The northern, interior radio peak has an apparently-associated mid-infrared filament. *NOTE: this figure was degraded in quality for distribution on astro-ph.*

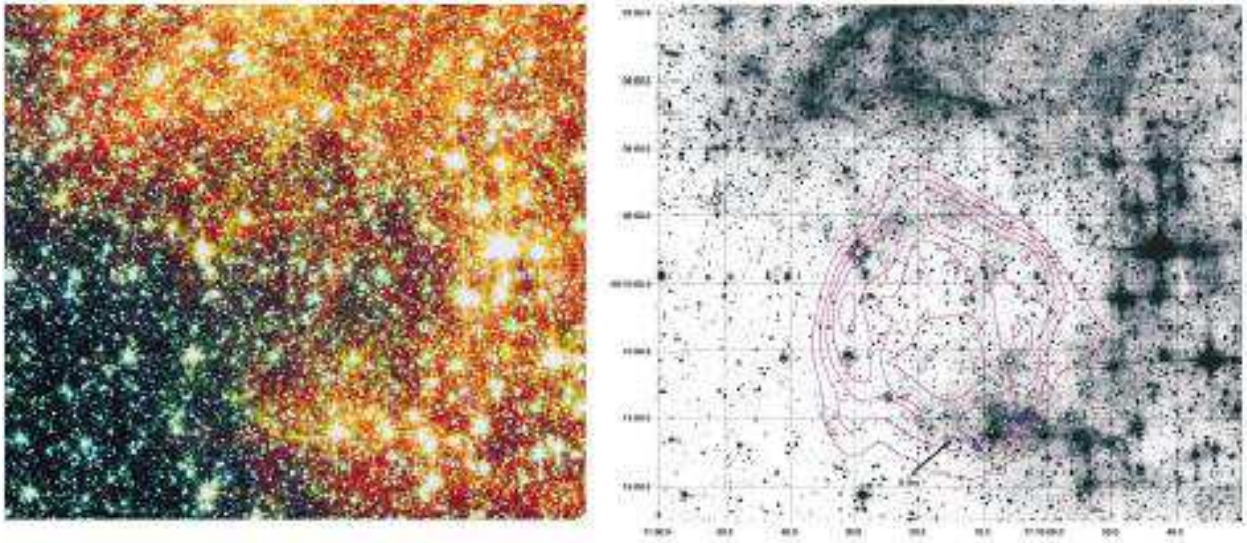


Fig. 19.— (a) *Spitzer*/IRAC color image of G346.6-0.2, with red= $8\ \mu\text{m}$, green= $4.5\ \mu\text{m}$, and blue= $3.6\ \mu\text{m}$. Radio contours from the MSC are overlaid in magenta; contour levels are 50, 100, 150, 200, 250 mJy/beam in a $43'' \times 67''$ beam. (b) *Spitzer*/IRAC $5.8\ \mu\text{m}$ image of G346.6-0.2 with radio contours (magenta) and the locations of OH 1720 MHz masers (blue diamonds) superposed. The greyscale ranges from 8 to 43 MJy sr⁻¹. *NOTE: this figure was degraded in quality for distribution on astro-ph.*

CTB 37A (G348.5+0.1)—Figure 20a shows patches and filaments of $4.5 \mu\text{m}$ (green) emission indicating shocked H_2 in the north, as well as patches and filaments of $5.8\text{--}8 \mu\text{m}$ (red) emission in the center and east of CTB 37A. The radio image has a ‘breakout’ morphology suggesting impact into a denser medium in the NE and less dense in the SW. The $5.8\mu\text{m}\text{--}8\mu\text{m}$ image (Fig. 20b) shows that the mid-infrared emission, probably from shocked gas, has a similar morphology. Green patches in the north correspond to the northernmost of the eight OH 1720 MHz masers with velocities around -65 km s^{-1} , which are associated with CTB 37A. None of the other maser spots in this remnant have associated $4.5 \mu\text{m}$ spots, though some faint, patchy emission is in the vicinity of most of the masers associated with CTB 37A. The patch of green mid-infrared emission in the NE is almost certainly shocked H_2 gas; the colors in IRAC channels (Table 2) are similar to that expected for $\text{H}_2\text{+CO}$ and not consistent with PAH emission. The red filaments in the IRAC image are clearly different, both in morphology and color. The arc near $17^{\text{h}}14^{\text{m}}14.7^{\text{s}}\text{--}38^{\circ}31'13''$ has IRAC colors $0.07/0.04/0.42/1$, consistent with PAH emission. Since there are so many regions with similar colors, it is possible that some of these red filaments are unrelated to the remnant. We suspect, however, that many of the infrared structures within the radio remnant are in fact related to the remnant. For example, the relatively bright, semicircular region including the filament mentioned above, the bright patch and associated filaments centered around $17^{\text{h}}14^{\text{m}}22.6^{\text{s}}\text{--}38^{\circ}35'06''$ are all located at the transition between the bright radio half-shell and the fainter extended emission that appears to be the opening of the blowout, probably near the surface of the pre-explosion cloud. Long filaments, especially visible in the $5.8\text{--}8 \mu\text{m}$ images, extend along the fainter NW and SW portions of the fainter, extended radio emission in the ‘blowout’ shell, accurately delineating the boundary. The colors of these extended filaments are consistent with PAH emission.

G348.5-0.0—This remnant is partially superposed on CTB 37A; high-resolution radio observations showed that G348.5-0.0 is a separate remnant (Kassim, Baum, & Weiler 1991). The Spitzer/IRAC image shows a narrow arc of emission that closely follows the radio rim. The correspondence between the $5.8 \mu\text{m}$ filament detected by IRAC (Fig. 20b) and the 6 cm radio rim detected with the VLA (Fig. 6 of Kassim et al. 1991) is precise, so the association of these features is beyond doubt. The filament is narrow—unresolved ($< 3''$) to IRAC. The filament is detected IRAC channels 2–4, with color ratios (Table 2) measured toward $17^{\text{h}}15^{\text{m}}04.6^{\text{s}}\text{--}38^{\circ}33'40''$. The $5.8/8 \mu\text{m}$ ratio is much too high to be PAH emission, and the filament is most likely dominated by emission lines from shocked gas. The radio extent of this remnant can be seen in sensitive VLA images (Kassim, Baum, & Weiler 1991) to extend across the NW part of CTB 37A and emerge from its northern rim. The second and third northernmost OH 1720 MHz masers in this region are at $V_{LSR} = -23$ and -21 km s^{-1} , clearly distinct from the velocities of the other 8 masers that are associated with CTB 37A.

There are also distinct molecular clouds at these velocities that are likely related to the remnants, with the -23 km s^{-1} cloud situated just west of G348.5-0.0 having the masers at its edge; this cloud is most likely associated with G348.5-0.0 (Reynoso & Mangum 2000). The Spitzer/IRAC images further support the idea that G348.5-0.0 is interacting with a dense cloud, because the infrared emission most likely traces relatively dense, shocked gas. The patch of green infrared emission in the northern part of CTB 37A is in the region where that remnant overlaps with G348.5-0.0 and could contain contributions from both remnants, but we associate it with CTB 37A based on the morphology (infrared filaments follow the CTB 37A radio shape, not G348.5-0.0, in this patch) and associated maser velocities. There is no infrared emission that appears related to the two OH masers associated with G348.5-0.0. The infrared filament along the radio rim of G348.5-0.0 is, however, clearly part of this remnant, and projecting it to the west, taking into account the curvature of the radio shell, it passes through the OH masers at -23 and -21 km s^{-1} . This remnant and CTB 37A are a special case of two different remnants interacting with two different molecular clouds, all superposed in the same several arcmin of the sky.

G349.7+0.2—This is one of the brightest SNRs in the survey, and owing to its great distance it is the most luminous. Its X-ray brightness makes it one of the most luminous X-ray remnants and it may be younger than 3000 yr (Slane et al. 2002). The radio image was constructed by combining VLA data in A, C, CD, and D configurations, with $5.0'' \times 2.1''$ resolution (Brogan et al. 2000). This remnant was shown to be interacting with a large molecular shell by Reynoso & Mangum (2001), and OH maser emission was detected by Frail et al. (1996). The mid-infrared emission is detected in all IRAC bands (Fig. 21); it is very bright at $5.8 \mu\text{m}$ and easily discerned at 4.5 and $8 \mu\text{m}$. There are 4.5 and $5.8 \mu\text{m}$ emission peaks near 4 of the 5 OH 1720 MHz maser spots (all except the first in Frail et al. (1996)); these peaks are not as prominent at $8 \mu\text{m}$. Shocked H_2 line emission is a likely contributor to the 4.5 and $5.8 \mu\text{m}$ wavebands. The $8 \mu\text{m}$ image may contain an emission mechanism in addition to the $\text{H}_2\text{S}(5)$ line, such as $[\text{Ar II}] 6.99 \mu\text{m}$. There is a filament of red (mostly $8 \mu\text{m}$) emission extending from the supernova remnant toward the west; it extends beyond the boundary of Figure 21 and has colors similar to other extended emission in the field nearby. This is apparently part of the dense cloud with which the supernova remnant is interacting. The unusual morphology of the remnant, with its shell much brighter on the western side, is caused by the shock propagating into the long axis of a roughly cylindrical cloud.

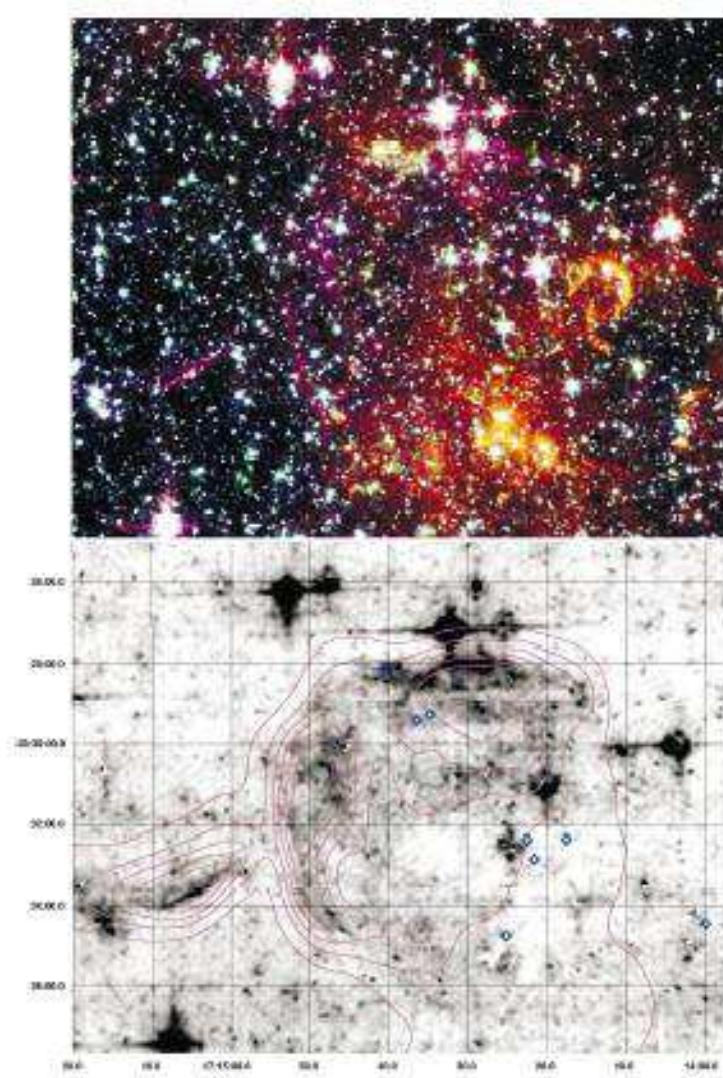


Fig. 20.— (a) *Spitzer*/IRAC $[5.8] - [8.0] \times 0.361$ image of the supernova remnants CTB 37A (G348.5+0.1) and G348.5-0.0. OH 1720 MHz maser positions (Frail et al. 1996) are overlaid as diamonds. No radio contours are overlaid, to avoid confusing the image, in which diffuse emission is evident from both SNR. CTB 37A is evident as a hemispheric shell including the relatively bright northern arcs at $17^{\text{h}}14^{\text{m}}35^{\text{s}}-38^{\circ}29'30''$ and western shell extending through $17^{\text{h}}14^{\text{m}}51^{\text{s}}-38^{\circ}31'50''$. G348.5-0.0 is evident as a short arc (labeled) passing through $17^{\text{h}}15^{\text{m}}05^{\text{s}}-38^{\circ}33'43''$. (b) *Spitzer*/IRAC color image of the supernova remnants CTB 37A (G348.5+0.1) and G348.5-0.0, with red= $8 \mu\text{m}$, green= $4.5 \mu\text{m}$, and blue= $3.6 \mu\text{m}$, magenta= $[5.8] - [8.0] \times 0.361$. The patch of green infrared emission in the NE is most likely shocked molecular gas where the blast wave is impacting very dense gas. This green patch contains the northernmost OH 1720 MHz maser, which is at -64.3 km s^{-1} (Frail et al. 1996) like most of the other masers that are associated with CTB 37A. G348.5-0.0 appears as a thin magenta filament (see Fig. 20 for a guide), suggesting ionic shocks. The western shell of CTB 37A is not as easy to see in this multi-wavelength image but has a magenta tint also suggesting ionic shocks. *NOTE: this figure was degraded in quality for distribution on astro-ph.*

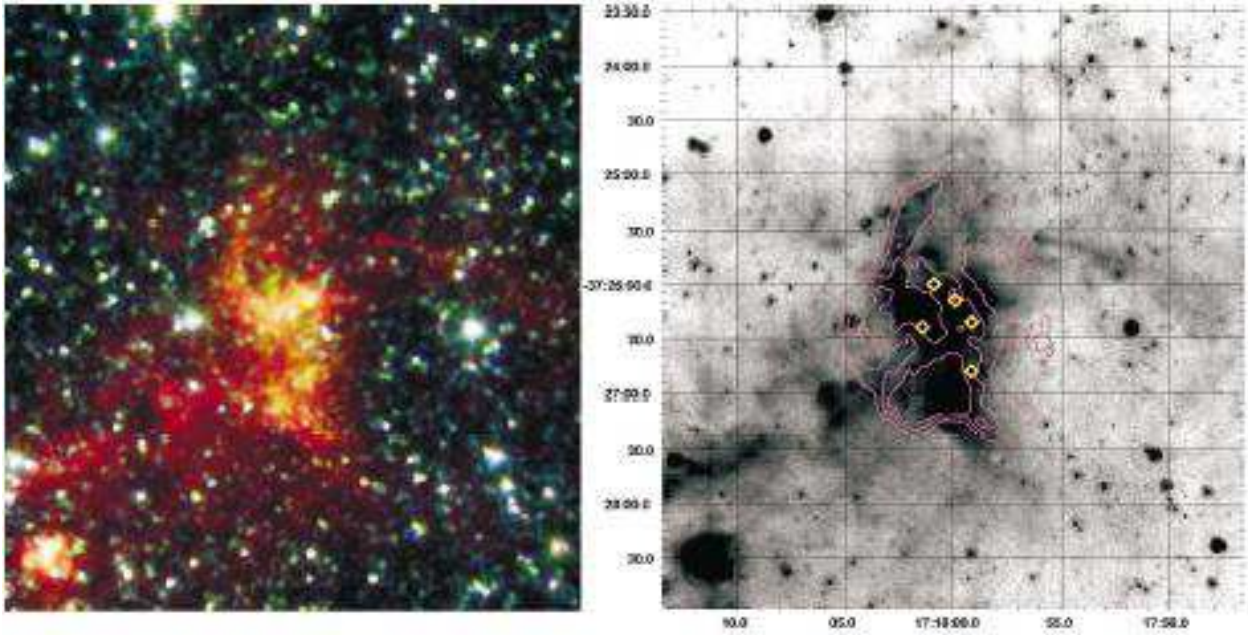


Fig. 21.— *Spitzer*/IRAC color image (left) and $5.8 \mu\text{m}$ image (right) of the supernova remnant G349.7+0.1. For the color image, red= $8 \mu\text{m}$, green= $4.5 \mu\text{m}$, and blue= $3.6 \mu\text{m}$, magenta= $[5.8] - [8.0] \times 0.361$. Radio 20-cm contours are overlaid on the channel 3 image. *NOTE: this figure was degraded in quality for distribution on astro-ph.*

5. Conclusions

The colors of the detected SNRs reveal a wide range of emission mechanisms. Figure 22 shows the observed colors for 1-2 spots per remnant together with bounding regions for molecular shocks, ionic shocks, and PAH emission from Figure 2. Nine spots have colors consistent with molecular shocks, 3 have colors consistent with ionic shocks, and 4 are consistent with PAH emission from unshocked ISM. Of the remaining all but one are intermediate between molecular and ionic shocks and probably represent a mixture of shock types. One spot, the Kes 69 ridge, falls sufficiently outside the bounds of emission mechanisms considered here that its colors cannot be explained by the mechanisms discussed here.

The SNRs with colors suggesting molecular shocks include 3C 391, Kes 17, G346.6-0.2, G311.5-0.3, G344.7-0.1, Kes 20 and G11.2-0.3. Two of these (3C 391 and G346.2-0.2) have associated OH 1720 MHz masers (Frail et al. 1996; Green et al. 1997). For comparison, only 14% of the entire sample of 95 remnants have OH 1720 MHz masers, so the association of these infrared colors with molecular shocks is not a chance coincidence. A total of 7 out of 18 IRAC-detected remnants have associated masers; the 39% association rate is again clearly not by chance. The remnants with colors suggesting molecular shocks but lacking OH masers may not have the specific, narrow physical conditions required to generate the maser inversions. For example, 3C 391 has a strong interaction with a giant molecular cloud on its bright radio NW ridge, but the OH masers are only present in two spots to the edge of the main interaction (Reach et al. 2002).

One of the remnants with IRAC colors in the ‘molecular’ region of the color-color diagram is the historical SNR G11.2-0.3. As discussed above, the mid-infrared emission from this young SNR may not be exclusively from molecular lines. Dust continuum is also unlikely to be the source of the unusual colors, because it would make the 8 μm band bright and move the colors to the left. Synchrotron radiation could contribute an extra source of 3.6 μm and 4.5 μm emission and could possibly explain the colors. Otherwise the colors could indicate unusual abundances; further spectroscopic observations are needed to understand this SNR.

The SNRs with colors suggesting ionic shocks are 3C 397, W 49B, and 3C 391 (NW ridge). The radio emission from all three is bright and highly structured, with bright near-infrared [Fe II] that correlates in detail with the radio structure.

The remnants with colors suggesting a mixture of molecular and ionic shocks are RCW 103, CTB 37A, G348.5-0.0, and 3C 396. In RCW 103, spectroscopy clearly reveals bright lines from both molecular and ionic shocks (Oliva et al. 1999). For CTB 37A and G348.5-0.0, OH 1720 MHz masers are associated suggesting likely shocked molecular gas.

The presence of both types of shock in an SNR is not unexpected, as the shocked dense clumps that cool via molecular lines are likely immersed in a lower-density medium that, when shocked, cools via ionic lines. This is clearly seen in the *ISO* spectra of W 28, 3C 391, W 44, IC 443, and RCW 103 (Reach et al. 2000; Oliva et al. 1999).

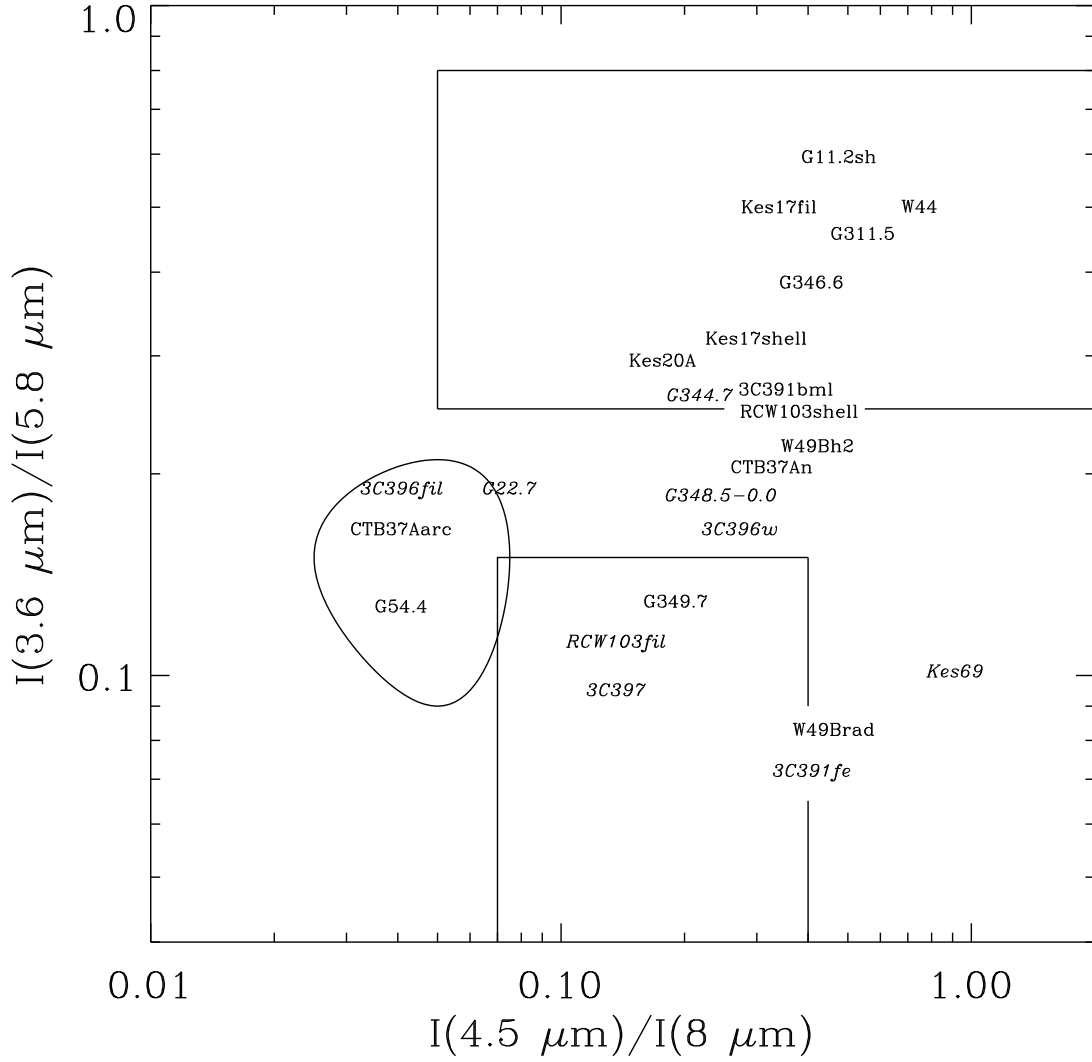


Fig. 22.— IRAC color-color diagram for 1 or 2 locations in each of the detected supernova remnants from this survey. The predicted colors of molecular shocks (upper rectangle), ionic shocks (lower rectangle), and PAH (circle) are copied from Figure 2 to aid interpretation. Labels are in *italics* for remnants with upper limits (generally, these are nondetections in channel 1 so the actual color would be *downward* from the label in this figure).

The details of the emission mechanism for each SNR remain to be determined with follow-up spectroscopy and comparison to ground-based observations. However, the IRAC survey already suggests a trend such that mid-infrared-detected SNRs tend to have colors suggesting shocks into dense gas. While this is an obvious selection effect, because many important cooling lines of such shocks are present in the mid-infrared, the sheer number of such detections suggests that molecular cloud interactions are not uncommon: at least 6% of SNRs in our survey show infrared colors suggesting molecular shocks. Some of these supernova remnants suspected suspected to be interacting with molecular clouds have been studied relatively little and await further investigation.

This work is based in part on observations made with the *Spitzer Space Telescope*, which is operated by the Jet Propulsion Laboratory, California Institute of Technology under NASA contract 1407. We thank Rick Arendt for his helpful comments.

REFERENCES

- Arendt, R. G. 1989, *ApJS*, 70, 181
- Arendt, R. G., Dwek, E., & Moseley, S. H. 1999, *ApJ*, 521, 234
- Benjamin, R. A. et al. 2003, *PASP*, 115, 953
- Brogan, C. L., Frail, D. A., Goss, W. M., & Troland, T. H. 2000, *ApJ*, 537, 875
- Brogan, C. L., Lazio, T. J., Kassim, N. E., & Dyer, K. K. 2005, *AJ*, 130, 148
- Burton, W. B. 1988, in *Galactic and Extragalactic Radio Astronomy*, eds. G. L. Verschuur and K. I. Kellermann (New York: Springer), p. 296
- Caswell, J. L., Kesteven, M. J., Stewart, R. T., Milne, D. K., Haynes, R. F. 1992, *ApJ*, 399, L151
- Chevalier, R. A. 1999, *ApJ*, 511, 798
- Condon, J. J., Cotton, W. D., Greisen, E. W., Yin, Q. F., Perley, R. A., Taylor, G. B., & Broderick, J. J. 1998, *AJ*, 115, 1693 (NVSS)
- Draine, B. T., & Lee, H. M. 1984, *ApJ*, 285, 89
- Dubner, G. M., Moffett, D. A., Goss, W. M., & Winkler, P. F. 1993, *AJ*, 105, 2251

- Enoguchi, H., Tsunemi, H., Miyata, E., & Yoshita, K. 2002, PASJ, 54, 229
- Fazio, G. G. et al. 2004, ApJS, 154, 10
- Fixsen, D. J., Moseley, S. H., & Arendt, R. G. 2000, ApJS, 128, 651
- Frail, D.A., Goss, W. M., Reynoso, E. M., Giacani, E. B., Green, A. J., & Otrupcek, R. 1996, AJ, 111, 1651
- Green, D. A., & Dewdney, P. E. 1992, MNRAS, 254, 686
- Green, A. J., Frail, D. A., Goss, W. M., Otrupcek, R. 1997, AJ, 114, 2058
- Green D. A., 2004, Bull. Astron. Soc. India, 32, 335
- Hwang, U., Petre, R., & Hughes, J. P. 2000, ApJ, 532, 970
- Jones, A. P., Tielens, A. G. G. M., & Hollenbach, D. J. 1996, ApJ, 469, 740
- Junkes, N., Fürst, E., Reich, W. 1992. A&A, 261, 289
- Kaspi, V. M., Roberts, M. E., Vasisht, G., Gotthelf, E. V., Pivovarov, M., Kawai, N. 2001, ApJ, 560, 371
- Kassim, N. E. 1992. AJ, 103, 943
- Kassim, N. E., Baum, S. A., & Weiler, K. W. 1991, ApJ, 374, 212
- Keohane, J., Reach, W. T., Rho, J. 2005, submitted.
- Lagage, P. O., Claret, A., Ballet, J., Boulanger, F., Cesarsky, C. J., Cesarsky, D., Fransson, C., Pollock, A. 1996, A&A, 315, L273
- McClure-Griffiths, N. M., Green, A. J., Dickey, J. M., Gaensler, B. M., Haynes, R. F., & Wieringa, M. H. 2001, ApJ, 551, 394
- Milne, D. K., & Dickel, J. R. 1975, Aust. J. Phys., 28, 209
- Moffett, D. A., & Reynolds, S. P. 1994, ApJ, 437, 704
- Olbert, C. M., Keohane, J. W., Arnaud, K. A., Dyer, K. K., Reynolds, S. P., & Safi-Harb, S. 2003, ApJ, L45
- Oliva, E. Moorwood, A. F. M., Drapatz, S., Lutz, D., & Sturm, E. 1999, A&A, 343, 943.

- Osterbrock, D. E. 1989. *Astrophysics of Gaseous Nebulae and Active Galactic Nuclei* (Mill Valley: University Science Books).
- Panutti, T., Rho, J., Reach, W. T. 2005, in preparation
- Patnaik, A. R., Hunt, G. C., Salter, C. J., Shaver, P. A., & Velusamy, T. 1990. *A&A*, 232, 467
- Reach, W. T., Rho, J.-H., 1996, *A&A*, 315, L277
- Reach, W. T., Rho, J.-H., 1998, *ApJ*, 507, L93
- Reach, W. T., & Rho, J. 2000, *ApJ*, 544, 843
- Reach, W. T., Rho, J.-H., Jarrett, T. H., & Lagage, P.-O., 2002, *ApJ*, 564, 302
- Reach, W. T., Rho, J.-H., Jarrett, T. H. 2005, *ApJ*, 618, 297
- Reach, W. T. et al. 2005, *PASP*, 117, 978
- Reynoso, E. M., & Mangum, J. G. 2000, *ApJ*, 545, 874
- Reynoso, E. M., & Mangum, J. G. 2001, *AJ*, 121, 347
- Rho, J., Petre, R., Schlegel, E. M., Hester, J. J. 1994, *ApJ*, 430, 757
- Rho, J.-H., & Petre, R. 1998, *ApJ*, 503, L1 67
- Rho, J., Jarrett, T., Cutri, R., & Reach, W. T. 2001, *ApJ*, 547, 885
- Rho, J., Reynolds, S. P., Reach, W. T., Jarrett, T. H., Allen, G. E., & Wilson, J. C. 2003, *ApJ*, 529, 299
- Rho, J. et al. 2005, in preparation
- Roger, R. S., Milne, D. K., Kesteven, M. J., Haynes, R. F., & Wellington, K. J. 1985, *Nature*, 316, 44
- Saken, J. M., Fesen, R. A., & Shull, J. M. 1992, *ApJS*, 81, 715
- Seward, F. D., Kearns, K. E., & Rhode, K. L. 1996, *ApJ*, 471, 887
- Seward, F. D., Slane, P. O., Smith, R. K., & Sun, M. 2003, *ApJ*, 584, 414
- Slane, P., Chen, Y., Lazendic, J. S., & Hughes, J. P. 2002, *ApJ*, 580, 904

Tam, C., Roberts, M. S. E. 2003, ApJL, 598, L27

Velusamy, T., Goss, W. M., & Arnal, E. M. 1986, J. Astron. Astrophys., 7, 105

Werner, M. W. et al. 2004, ApJS, 154, 1

Whiteoak, J. B. Z., & Green, A. J. 1996, A&AS, 118, 329 (MSC)

Yusef-Zadeh, F., Wardle, M., Rho, J., & Sakano, M. 2003, ApJ, 585, 319